PELLET ABLATION
IN THE
W VII-A STELLARATOR

Klaus P. Büchl
W VII-A Team*, NI Team**, and ECRH Team***

IPP 1/238 December 1986

MAX-PLANCK-INSTITUT FÜR PLASMAPHYSIK
8046 GARCHING BEI MÜNCHEN

MAX-PLANCK-INSTITUT FÜR PLASMAPHYSIK

GARCHING BEI MÜNCHEN

PELLET ABLATION IN THE W VII-A STELLARATOR

Klaus P. Büchl

W VII-A Team*, NI Team**, and ECRH Team***

IPP 1/238 December 1986

* G. Cattanei, D. Dorst, A. Elsner, V. Erckmann, U. Gasparino, G. Grieger, P. Grigull, H. Hacker, H.J. Hartfuß, H. Jäckel, R. Jaenicke, J. Junker, M. Kick, H. Kroiss, G. Kuehner, H. Maaßberg, C. Mahn, G. Müller, W. Ohlendorf, F. Rau, H. Renner, H. Ringler, F. Sardei, M. Tutter, A. Weller, H. Wobig, E. Würsching, M. Zippe.

** K. Freudenberger, W. Ott, F.P. Penningsfeld, E. Speth.

*** W. Kasparek, G.A. Müller, P.G. Schüller, M. Thumm, R. Wilhelm (Inst.f.Plasmaforschung, Univ.Stuttgart).

Die nachstehende Arbeit wurde im Rahmen des Vertrages zwischen dem Max-Planck-Institut für Plasmaphysik und der Europäischen Atomgemeinschaft über die Zusammenarbeit auf dem Gebiete der Plasmaphysik durchgeführt.

PELLET ABLATION IN THE W VII-A STELLARATOR

Klaus P. Büchl
and
W VII-A-, NI-, and ECRH-Team

IPP 1/238

Abstract

Pellets of different sizes (0.6, 0.8 and 1.0 mm ϕ) are injected into stellarator plasmas with ohmic, ECR, and neutral injection heating. The direct particle deposition inside the plasma was incomplete for large pellets with total penetration and for ECRH plasmas generally. In NIH plasmas the total mass of the pellets was deposited and the density rise without increase of impurities resulted in energy contents of 4.8 kJ which exceeds the values for gas-fuelled discharges: Radiation fluctuations during pellet ablation are also observed in a stellarator for the first time.

1. Introduction

Pellet injection experiments have mostly been performed in tokamaks [1], but a few have been conducted in other devices. Besides in Puffatron [2], pellets have been used in the W VII-A and Heliotron E [3] stellarators. The main objective in injecting pellets into W VII-A was to improve the target plasma for neutral beam heating. With pellets it was possible to achieve higher plasma density and produce it faster than it was with gas puffing. This led to better absorption of neutral beam power and thus to faster plasma energy build-up. These results are described in [4] and will be mentioned briefly in the relevant sections. This report is mainly concerned with giving a detailed description of pellet ablation in different stellarator discharges. A short review of the pellet injector and the diagnostics used is followed by sections on ablation in OH, ECRH, and NIH plasmas. A further section describes fluctuations observed in the ablated plasma. They occur in similar form in tokamak experiments.

2. Pellet Injector

Deuterium pellets are injected into WVII-A (Fig. 1) with a single-shot pneumatic gun. The injector is described in detail in [5]. A hydrogen gas pressure of 0.5 MPa to 3.0 MPa accelerated the pellets up to velocities of 400 m/s to 1000 m/s. The pellets are cylindrical in shape. The length of the pellets is equal to their diameter. Three sizes are applied: 0.6 mm, 0.8 mm, and 1.0 mm (Fig. 2). The pellets are radially injected into the torus. Because the plasma in a stellarator is non-circular in shape, the pellets do not enter the flux surfaces perpendicularly. In the pellet injection plane the plasma cross-section is elliptical and the axes of the ellipses form angles of 45° to the pellet trajectory.

3. W VII-A Stellarator and Diagnostics

W VII-A is a shear-free $\ell = 2$ stellarator with a toroidal field of 1 – 3.5 tesla. The rotational transform was in the range of 0.1 – 0.6. The major radius of the torus is 200 cm, the minor radius 10 cm. The stellarator is described in detail elsewhere [6].

The pellets were injected in three different heating regimes:

- ohmic heating (OH) with a toroidal current of 20 kA ("tokamak" regime).
- ECR heating (ECRH) with a power of 200 kW at 70 GHz or 28 GHz.

- NI heating (NIH) with a power of 1 MW by beams with nearly perpendicular injection (6°). The neutral-beam-heated plasma was developed either from an ohmically heated plasma by decreasing the current or from an ECRH plasma.

The standard stellarator diagnostics used for measuring of the ablating pellet were a one-channel IR interferometer, a diamagnetic loop, a XR diode array, and single-point Thompson scattering. The XR diode array was located in the pellet injection plane during the early experiments (OH and NIH plasmas) and viewed the pellet directly (Fig. 3). Later the pellet injector was moved to another poloidal plane. Additional information was gained from ECE measurements, spectroscopy and bolometry. The ablation of the pellet was observed directly by means of an H_α diode and time-integrated photography. The pellet velocity was also calculated from signals of light barriers for each shot.

From photography of the ablation trace and H_α measurements it was possible to determine the penetration of the pellets and obtain information on particle deposition. The XR array allow the penetration of the pellet and excitation of modes to be observed. The IR interferometer measurements were used to estimate the mass deposited. The diamagnetic loop and Thomson scattering make contributions to the question of the adiabatic response of the plasma.

4. Pellet Injection into OH Plasmas

The plasma in the stellarator was produced by a toroidal current of 20 kA with a flat-top time of 300 ms. The toroidal magnetic field was 3.5 tesla. The external rotational transform was 0.12. Including the poloidal field of the ohmic current, a tokamak-like ι profile was produced. Deuterium pellets of 1.0 mm ϕ and 1.0 mm length were injected into this discharge with a velocity of 500 to 600 m/s. The total number of deuterium atoms contained in a pellet was estimated at $3.4 \cdot 10^{19}$.

The approximate number of deposited atoms N_{dep} is calculated from the measurements of the IR interferometer. For a plasma radius of 10 cm we obtain

$$\Delta\bar{n} = 0.05 \cdot \Delta \int n \cdot d\ell|_{exp}$$

$$N_{dep} = 2\pi^2 r^2 R \Delta\bar{n}$$

$$N_{dep} = 3.95 \cdot 10^5 \cdot \Delta\bar{n}$$

Errors due to miscounting of the fringe counter can often be corrected if one follows the fringe shift backward in time from the end of the discharge. A typical interferometer

trace is shown in Fig. 4. The discharge will not disrupt although there are 300% as many injected particles as particles in the plasma. Values of the instantaneous density rise and deposited atoms are determined from several shots:

$$\Delta\bar{n} = 2.1 \cdot 10^{13} - 5 \cdot 10^{13}\,\mathrm{cm}^{-3}$$

and

$$\overline{N_{dep}} = 0.8 \cdot 10^{19} - 2 \cdot 10^{19}\,\mathrm{atoms}$$

These are 25–50% of the atoms in the pellet. The conclusion that only part of the pellet is ablated inside the plasma is also supported by H_α and XR measurements.

During ablation of the pellet H_α emission was measured (Fig. 5) by viewing the trace with a photomultiplier. With a velocity of 500 m/s the pellet penetrates the plasma column in 400μs, but the measured H_α signal lasts about twice as long. This can be interpreted in the following way: the pellet is not completely ablated inside the plasma; its remaining core hits the inner wall of the torus, is evaporated by the impact and produces a strong gas puff. The gas emits line radiation during ionization at the plasma edge, which will be observed directly by the H_α detector viewing along the pellet trajectory.

The pellet is also seen in the plasma by the XR array (Fig. 6). Interpretation of the XR signals in detail is difficult, but an increase means mainly density increase and decrease is mainly due to temperature drop. The elliptical shape of the plasma column and impurity radiation should also be taken into account. The initial increase of the XR signals outside about a/2 could be produced just by the local density increase as well as by impurity line radiation emitted from the cooled plasma. However, when the pellet intersects a radius near a/2, which is probably identical with the q=1 surface, the radiation simultaneously decreases inside this radius, presumably owing to the temperature drop, and increases in the outer plasma layers at the same time. The X-ray emission in the outer channel is larger than in the corresponding inside channels. Because it is also moving towards the axis it should be generated by the initial deposition. However, the signals of the channels near the inside wall rise simultaneously at the same time when the central signals drop. This gives the impression that no toroidal transport of the deposited mass occurs up to this time. This very fast process can be seen at all radii and its estimated velocity is faster than 10^6cm/s. It is possible that the deposited cold plasma cloud distorts the field configuration so that energy transport along the field lines to the outside can occur. After the pellet has passed through the whole plasma, the channels of the XR array near the inner wall see an increase in radiation, which could be due to "gas puffing" by the residual pellet. But the rise could als be generated

by impurities entering the plasma. On photographs made during pellet injection in NIH discharges bright-bluish traces of wall particles can be seen when the pellet hits the inner wall of the torus (Fig. 29).

In agreement with these observations, calculations of pellet ablation using the neutral gas shielding model result in total penetration of 1 mm pellets with a velocity of 400 m/s through a plasma of electron temperature of 500 eV and electron density of $5 \cdot 10^{13}\,\mathrm{cm}^{-3}$.

Is the ablation of the pellet in the plasma an adiabatic process or will energy losses occur? The measurement of the plasma energy will show the energy drop due to transfer of energy into ionization and dissociation of the pellet material. If there are no other losses, the ablation will be called adiabatic. The electron temperature and density on axis were determined by Thompson scattering on a shot-to-shot basis before and after pellet injection (Fig. 7). While on axis the density rose by a factor 2.5 and the temperature dropped by 3.5. The averaged energy loss of about 320 J was in agreement with the measurements by the diamagnetic loop, which result in losses between 200 J and 400 J. An energy loss of several hundred J was also measured with the bolometers. The energy loss during ablation due to ionization, dissociation, radiation, and charge exchange is given by

$$\Delta E_{ion} = \varsigma \cdot E_i \cdot N_{dep}$$

E_i is the ionization energy of deuterium. The factor ς includes the losses due to dissociation, radiation, and charge exchange. We shall assume $\varsigma = 2$. We then get

$$\Delta E_{ion} = 5.0 \cdot 10^{-18} \cdot N_{dep}$$

and

$$\Delta E_{ion} \approx 40 - 80\,\mathrm{J}$$

Because the measured energy loss of about 300 J is a factor of 10 as large as that expected, we can conclude that in these experiments the ablation and associated processes are not adiabatic. The fast energy drop seen inside the plasma by the XR signals may indicate the process responsible for the energy loss.

The electron temperature profile before and after pellet injection was measured by ECE diagnostics. The temperature recovers by ohmic heating within 20 ms but the profile shape has already recovered in 4 ms (Fig. 8). This is in good agreement with observations in tokamaks. The temperature profiles in, for example, ASDEX return to their pre-pellet shape within periods of the order of a millisecond.

Can the energy content of the plasma be increased by pellet injection? After the instantaneous deposition of pellet particles, the density drops within about 10–20 msec to a slowly varying density level (Fig. 4). At higher start densities ($\bar{n} \approx 4 \cdot 10^{13}\,\mathrm{cm}^{-3}$) this level is only slightly above the density before pellet injection. At medium initial densities ($2-3 \cdot 10^{13}\,\mathrm{cm}^{-3}$) a gain of $1 \cdot 10^{13}\,\mathrm{cm}^{-3}$ is obtained. At lower densities a gain of this order is often reached without the sharp density peak at the time of deposition. For shots with an ohmic current of 20 kA it was not possible to exceed a quasi-stationary density of $4-5 \cdot 10^{13}\,\mathrm{cm}^{-3}$; the density also peaks to $7 \cdot 10^{13}\,\mathrm{cm}^{-3}$ during injection. At toroidal currents of 30 kA flat top density levels $6 \cdot 10^{13}\,\mathrm{cm}^{-3}$ could be reached. The total energy content of the plasma measured by the diamagnetic loop during the density flat top is shown as a function of the mean plasma density in Fig. 9. The points for pellet-fuelled OH discharges are slightly above those for gas-fuelled discharges at the same density, but no significant increase is observed. Equivalent gas-fuelled discharges and pellet-fuelled discharges (after reheating) contain equal energy contents for the same density. Influence of the pellets on the transport is not recognizable. However, pellet filling could be advantageous with respect to impurities. In gas-fuelled discharges the impurity content rises simultaneously with the plasma density. Pellet injection makes the hydrogen density jump to a higher level without immediate changing the impurity content. The plasma can therefore be sustained at a higher density for a longer time before the increasing radiation losses terminate the discharge.

5. Pellet Injection Into ECRH Plasmas

ECRH plasmas are produced in the stellarator for use as target plasmas for further heating by neutral beam injection. The plasmas created have mean electron densities of $0.5-1.5 \cdot 10^{13}\,\mathrm{cm}^{-3}$ and electron temperatures on axis of about 1000 eV. The absorption of neutral beams is rather inefficient at these low densities. Increasing the density by means of pellets could make the absorption more effective. It is known, however, that ECRH produces suprathermal electrons, to which pellet ablation is very sensitive. The deposition of the pellet material inside the plasma thus has to be determined. In most of our injection experiments the ECRH plasmas are produced by RF of 70 GHz and 200 kW. Pellets of 0.6 mm ϕ and 0.6 mm length are injected at velocities of about 600 m/s.

The number of particles deposited is estimated from IR interferometer measurements (Fig. 10). The mean deposition from several shots is

$$\overline{\Delta N}_{dep} = 2.6 \cdot 10^{18}\ \text{atoms}$$

A pellet contains approximately $N_{pel} = 8 \cdot 10^{18}$ atoms, which is equivalent to 400% of the plasma particles. About 30% of the pellet is deposited in the plasma. The penetration depth d_p of the pellets was determined from photographs (Fig. 28). Unlike in OH discharges, pellets penetrate the plasma just to the axis: depth $d_p \approx 10$ cm. The conclusion is that a large part of the pellet is already evaporated near the edge before entering the inner part of the plasma. The remaining core of the pellet travels into the plasma and is ablated inside. This assumption is in agreement with calculations of pellet ablation using the neutral gas shielding model. Pellets containing $6 \cdot 10^{18}$ atoms or more should penetrate the plasma totally (Fig. 11a). However, pellets with a content of $2.3 \cdot 10^{18}$ atoms, which is equivalent to 30% of the initial pellets, should go just to the axis of the discharge (Fig. 11b).

The energy for dissociation, ionization etc., ΔE_{ion}, is calculated from the number of atoms in the pellet. For the total pellet one gets 40 J. If we use the number of atoms deposited, we obtain 15 J. The drop in the energy content of the plasma measured by the diamagnetic loop ranges from $<$ 10 J to 60 J. For shot # 63012 (Fig. 10), for example, the immediate energy drop is 18 J. In ECRH plasmas the ablation is an adiabatic process. There is no evidence of a drastic energy loss during pellet injection.

Electron temperature profiles are measured by ECE diagnostics. As in OH discharges, the temperature profile (Fig. 12) returns to its pre-pellet shape within 2–3 ms, while the temperature on axis recovers in about 10 ms. The energy content of the plasma has risen during reheating because the density is still high. In Fig. 9 the energy content is shown as a function of density. The energy content of ECRH plasmas is below that of OH plasmas, with and without pellets. However, for ECRH plasmas pellets extend the density range and therefore the energy content to larger values. The life history of an ECRH plasma with pellet injection (Fig. 13) also shows the extension of the density range and the transition to higher energy content. The discharge starts in the pre-pellet region at low density and low energy content. The pellet causes the plasma to jump immediately to higher density at almost constant energy content apart from an initial small drop due to ionization. The energy content then subsequently grows at nearly constant density by heating until the post-pellet region is attained. The plasma decay into the pre-pellet region follows the history of gas-fuelled ECRH discharges.

Generally after pellet injection the energy content recovers very fast, but in some discharges the recovery time is significantly slower (Fig. 14). A comparison of bolometer measurements is the two cases is shown in Fig. 15. A very slow recovery of the total energy content to its pre-pellet level (20 ms) is observed in discharges with a dramatic increase of the total radiated power after pellet injection. Examples are shots

63003 and # 63006 (Fig. 15b). However, in discharges like shot # 63012 (Fig. 10) the energy content achieves its pre-pellet level in less than 3 ms and keeps rising. It exceeds this level proportionally to the density by a factor of 3. In these discharges the total radiated power increases just moderately after pellet injection (Fig. 15a). These plasmas do not become radiation-dominated and are thus able to attain high energy contents.

The injection of 0.8 mm pellets into plasmas heated by ECR at 28 GHz is also strongly influenced by fast electrons. In contrast to the injection of smaller pellets at 70 GHz, the density rise is not instantaneous. The line density increases in about 2 ms as for gas puffing. The number of atoms deposited in the plasma as measured by the IR interferometer is 5-10% of the content of the pellet. The H_α signal lasts much longer than $300\mu s$ on a low level comparable to that of a fast gas puff, but the peak in front has a duration of $100\mu s$ (Fig. 16). In accordance with the pellet velocity of 400 m/s the pellet penetrates 4 cm into the plasma in $100\mu s$. This agrees roughly with the penetration depths calculated from the neutral gas shielding model if the number of deposited atoms is used for the calculation, i.e. the pellet enters the plasma with reduced size.

The assumption suggested is as follows. The pellets will be partly ablated by fast electrons near the edge of the plasma. The presence of suprathermal electrons in ECRH plasmas is confirmed by ECE measurements for RF heating of 28 GHz as well as 70 GHz. To get an estimate of the number of suprathermal electrons necessary to ablate the pellet, we consider the energy balance:

$$k \cdot f \cdot \overline{E_{fe}} \cdot N_{fe} = (N_{pel} - N_{dep}) \cdot \varsigma \cdot E_i$$

N_{fe} number of fast electrons in the plasma

$\overline{E_{fe}}$ mean energy of fast electrons (30 keV)

N_{pel} atoms contained in the pellet

E_i ionization energy of deuterium (13.6 eV)

k part of the energy of a fast electron used for ablation (≈ 1)

f geometry factor, percentage of fast electrons absorbed from the pellet (≈ 0.05)

ς energy factor per ionization (≈ 2).

From this equation using the measured N_{dep} the number of fast electrons in the plasma is estimated to be

$$N_{fe} \approx 1 \cdot 10^{17} \text{ electrons}$$

This is about 1% of the electrons contained in the plasma. in agreement with estimations from ECE measurements. To ablate 90% of the pellet, only $5 \cdot 10^{15}$ suprathermal electrons would be necessary.

6. Pellet Injection into NIH Plasmas

Currentless plasmas for heating by neutral injection are produced in the W VII-A stellarator in two ways. The first method starts from an ohmically heated plasma, such as a tokamak plasma with a toroidal current of about 20 kA. The current will then be decreased while the total rotational transform is kept constant, by increasing the external rotational transform at the same time. This plasma will act as a target for neutral beam injection. The second method is ignition and creation of the target plasma by applying electron cyclotron resonance heating of 200 kW at 28 GHz or 70 GHz. The neutral beams are directed nearly radially into the plasma column. Unlike in tangential injection used in other machines, only a small part of the beam energy is absorbed depending on the plasma density. Pellet injection could be a good method to increase the plasma density and thus enhance the energy absorption. This is especially true of low-density ECRH discharges. Pellets were fired in both types of discharges during neutral injection heating. Most of the experiments used D_2 pellets of 0.6 mm ϕ ($N_{pel} \approx 7 \cdot 10^{18}$), but some investigations were done with 0.8 mm ϕ pellets ($N_{pel} \approx 2 \cdot 10^{19}$) and also with 1.0 mm ϕ pellets ($N_{pel} \approx 3.4 \cdot 10^{19}$). The pellet velocity was between 400 and 700 m/s.

Estimation of the deposited mass of the 0.6 mm ϕ pellets using the IR interferometer yields the entire mass of the pellet. In contrast, for the 0.8 mm ϕ pellets just 30–50% of the total mass was detected in the discharge. The latter is in agreement with the photography of the ablation trace (Fig. 17), which shows total penetration of the 0.8 mm ϕ pellet through the plasma column. This means that only part of the pellet mass is deposited inside the plasma. The rest hits the inner wall of the torus, vaporizes and acts like a short gas pulse, increasing the edge density. In this particular shot traces of sputtered wall particles can also be seen. The photos are taken with a time-integrated camera. The shutter is opened during the whole duration of the discharge. One cannot decide therefore whether the wall particles are produced as a result of the pellet impact or during the end of the discharge.

Measurements of the electron temperature T_{eo} and electron density n_{eo} at the axis were made by laser scattering (Fig. 18). In these experiments pellets 1 mm in diameter containing $3.4 \cdot 10^{19}$ deuterium atoms were applied. The density calibration is made from the IR interferometer measurements. Before pellet injection we get $\int ndl = 1.0 \cdot 10^{15}\,\mathrm{cm}^2$. If we assume a parabolic density profile, the pre-pellet density on axis is $7.5 \cdot 10^{13}\,\mathrm{cm}^{-3}$. From Thomson scattering the number of deposited atoms is estimated to be $1.0 \cdot 10^{19}$, i.e. 30% of the pellet. From the step in line density one calculates $N_{dep} = 3.0 \cdot 10^{18}$ for a parabolic profile. This is only 10% of the 1 mm ϕ pellet. Like 0.8 mm ϕ pellets, the 1.0 mm pellets penetrate the plasma totally and deposit even less of their masses than 0.8 mm pellets. The expected energy loss for ionization etc. of the deposited particles is $20 - 50$ J, depending on N_{dep}. The measurement of the diamagnetic loop gives an energy drop of this order of magnitude. However, from Thomson scattering we estimate an energy loss of 200 J. This means that during or shortly after pellet injection the plasma is losing energy. After 2 ms the plasma has already reached its pre-pellet value of energy content. In OH discharges the energy is recovered in 15–20 ms. The fast reheating of the plasma by NIH is probably due to interaction with the ions from the beam injection.

Pellet injection increases the absorption of neutral beams. This is evident from Fig. 19. The target plasma is produced from an ohmic discharge. The power of the neutral beams is 1.7 MW. Before injection of 0.6 mm pellets the total energy content rises at a rate of 30–50 kJ/s. Then for 5–8 ms when the temperature recovers, the rate changes to 120–160 kJ/s. Later the rate again drops to 30–50 kJ/s. The subsequent slow decrease of the energy content may be caused by increased radiation losses. Energy contents will therefore be higher if the pellet injection occurs earlier in time. Up to 3400 J was measured in these experiments. It turns out that the advantage of pellet injection is the density rise without direct enhancement of impurities.

During a discharge the total energy content develops from a low level to a higher level, depending on the density. In Fig. 20 the life histories of two shots are shown. Both discharges start in the pre-pellet region. The density of shot # 34420 without pellet increases owing to deposition of the neutral beam. The energy rises proportionally to the density to almost 3 kJ. The line density of shot # 34469 jumps during pellet injection to $8 \cdot 10^{14}\,\mathrm{cm}^{-2}$, while the energy content is constant. Subsequently, the energy is strongly increased by heating. The density changes as a result of deposition of beam particles. The plasma achieves a maximum energy content of nearly 5 kJ in the post-pellet region at the end of NIH. The decay of the plasma starts by rapid cooling without loss of particles because of the good confinement. From the history of the gas-fuelled

discharge in Fig. 20 one can extrapolate that the energy content would also attain the post-pellet region. For that case the density will be increased by gas puffing alone.

Good and bad confinement for non-rational and rational values of the rotational transform ι(a) can be impressively demonstrated by pellet injection (Fig. 21). After pellet injection the density contines to be high in NIH plasmas with good confinement (e.g. ι (a) = 0.45) and increases more owing to deposition of the neutral beams. Moreover, the basic rate has gained because of the higher absorption of the beams of higher densities. The density decay time, which is a measure of the particle confinement time, is substantially longer than the discharge duration of about 100 ms. However, the density decays to the non-pellet level in about 30 ms indicating a considerable reduction in particle confinement time, if the rotational transform ι(a) is a rational number, e.g. 1/3.

In beam-heated ECRH target plasmas the absorption of neutral beam energy also increases with density (Fig. 22). As in OH target plasmas, the energy content rises at a rate of 30–50 kJ/s before the pellet. During reheating this rate goes up to 100 kJ/s. The maximum total energy obtained again depends on the time of pellet injection at a given rotational transform ι. An energy content of up to 2000 J was measured.

A vertical 30-channel XR array was located in the plane of pellet injection. The time resolution was set at $10\mu s$ for pellet observation. Large signals are observed in all channels during and subsequent pellet injection. However, interpreting them in terms of density and temperature is difficult for pure hydrogen plasmas, but even more difficult when impurity radiation is included. We can assume that the high density of the cold plasma cloud around the pellet, of the order of $10^{17}\,\mathrm{cm}^{-3}$,causes a rise in the XR signal. We can also assume that an observed drop of the XR signal can be interpreted as a temperature drop if in this volume the density does not change much. Figure 23 gives an example of an XR measurement during pellet injection. The large positive signals increasing from the edge to a maximum at r = 3 cm and then decreasing can be interpreted in terms of particle deposition on the pellet path. There is no positive peak at the corresponding radius of the inside channels. No large density rise is expected at the inner points, because the deposited material arriving is already distributed over the entire flux surface. If a small density rise is hidden in the inside XR signals, it cannot be detected. The negative signals at the inner radii may be caused by a temperature drop. This drop happens when the signals in the corresponding outer channels have a large peak due to the density deposition. Profiles obtained from the XR signal are shown in Fig. 24 for three times. The time is counted as of the first identified change of the diode signals, when presumably the pellet crosses the plasma edge. The scale of the negative ordinate is enlarged. The propagation of the pellet towards the axis is clearly

indicated. The toroidal flow of the ablated material after ionization decreases the very high density near the pellet trajectory, as can be seen in the XR profile at $220\mu s$. A typical flow velocity of a few 10^6 cm/s can be estimated from the "density" drop from $100\mu s$ to $500\mu s$ and the circumference of the stellarator of about 12 m.

7. Pellet Injection into Plasmas with Combined ECRH and NIH

Pellets 0.8 mm in diameter were injected into a plasma heated simultaneously by neutral beams and ECR of 28 GHz (Fig. 25). These experiments were not successful in spite of the increase in the total energy content of the plasma. As a result of pellet injection, the plasma loses most of its energy. In general, the results are very similar to those of the experiments with ECRH (28 GHz) alone which were described above. The density rises slowly in about 2 ms, which is typical of a fast gas puff, and only 5 – 10% of the pellet will be found in the plasma. If we take into account only the fast density rise in less than 1 ms, then the mass deposition by ablation inside the plasma is about half of this. A penetration depth of 5 cm can be estimated from H_α measurements (Fig. 26). H_α emission with lower intensity for several ms indicates continuing gas influx after pellet injection. The measurements can be explained by the assumption of suprathermal electrons with energies of between 10 and 100 keV. During ECRH the generation of suprathermal electrons in these plasmas is well observed by ECE diagnostics. These electrons will cause strong and rapid ablation of the pellet near the edge of the plasma. We conclude that the ablation in plasmas with simultaneous ECRH and NIH is dominated by wave heating.

8. H_α Fluctuations during Pellet Ablation

Time-integrated photos of the ablation of pellets were taken perpendicularly to their trajectory, as shown in Fig. 1. The explanation and scaling of the photos are given in Fig. 27. The injection of 0.6 mmϕ pellets into ECRH plasmas (Fig. 28) and of 0.8 mm ϕ pellets into NIH plasmas (Fig. 29) is imaged. The pellets in Fig. 28a–c penetrate to the axis of the stellarator. The dense plasma cloud produced extends in the toroidal direction symmetrically to the two sides. The expected penetration depth calculated by the neutral gas shielding model (see Fig. 11b) is in agreement with the observations. We assume that the light emission is proportional to the deposition rate. A monotonic increase in brightness from the edge of the plasma to the centre will therefore be expected. Figure 28a (#63015) comes close to this. However, a structure

perpendicular to the toroidal direction is observed in most of the photos. These emission fluctuations are less marked in the first part of the trajectory but are very strong in the second part near the maximum emission. If the photos are taken with a larger aperture (Fig. 28 c–d) the pellet path can be seen directly as a white line which is slightly curved in the toroidal direction. Pellets can penetrate the plasma totally if their mass or velocity or both is somewhat increased (Fig. 28d). The ablation between the plasma axis and the inner wall is strongly reduced, because the pellet crosses flux surfaces, whose temperatures are already decreased. In contrast to the small pellets injected into ECRH plasmas, pellets of 0.8 mm ϕ shot into NIH plasmas penetrate completely (Fig. 29). The blue-violet colour of the discharge may arise from impurities. The emitted light shows very strong fluctuations. Beyond the plasma axis the ablation is again reduced, but fluctuations can still be observed. It is also conspicuous that the plasma flow does not seem to extend so far in the toroidal direction before getting completely ionized. These features may be related to heating by fast ions.

There might be different reasons for the fluctuations, as can be imagined. Hot spots on the pellet, for example, would give random bursts of ablation. But then one should observe jets and no symmetry in the toroidal direction. The fluctuations should also become smaller when the lifetime of the pellet decreases. But the measurements, especially the H_α signals, show the opposite: increasing fluctuations with time. An indication that these fluctuations are coupled with the magnetic field is provided by a pellet which breaks into three parts (Fig. 30). After the traces have divided, the fluctuations of ablation are still synchronized. Later on the coincidence is lost, but the tracks may no longer be in the same horizontal plane. One could imagine a fast developing instability which forms rolls as in clouds or the Rayleigh instability of a liquid jet. However, the synchronization of the ablation of fragments may be hard to explain. The fluctuations could be produced by variations in the energy available for ablation in different flux surfaces. When the fluctuation phenomenon was first discovered in ASDEX [7], it was speculated that it could depend on rational q-values. In these flux surfaces only a limited content of energy is available for ablation of the pellets. But in a stellarator the rotational transform does not change that much. It varies a little owing to beta and current effects, but not in a wide range. Nor do the fluctuations seem to be reproducible, but this is hard to say from the photos. Another explanation of the fluctuations might be the shielding of the pellet by the cold, dense and partially ionized plasma cloud. If more material is ablated, the cloud gets denser and needs more energy for ionization. The ablation should thus decrease. When the cloud has been ionized and expanded, more of the energy should go to the pellet surface and ablation should increase. The motion of the pellet should also be taken into account. This could explain the experimental

observation that the fluctuations seem to be proportional to the local ablation. If the ablation is small at the beginning of the pellet track, the fluctuations are also small. If the ablation is large far inside the plasma, the fluctuations are also large. A scenario like this might also be possible, but it has not been worked out yet. The decision which of the models correctly describes the observed fluctuations presumably requires more experiments.

Conclusion

A summary of the pellet injection experiments in the stellarator is presented in Table 1. One of the main difficulties of the experiments was the proper choice of the pellet size. Mostly, 1.0 mm ϕ and 0.8 mm ϕ pellets were too big and they are not totally ablated inside the plasma. They penetrate the plasma column, and the core of the pellet hits the inner wall. In several shots enhanced plasma losses and disruptions thus occur as a consequence of pellet injection. In surviving plasmas the effect of inner deposition cannot be clearly studied because of the influence of the fast gas pulse from the unablated rest of the pellet. In contrast to the experiments with 1.0 and 0.8 mm pellets, the experiments using 0.6 mm pellets are very successful.

In ECRH plasmas strong influence due to the presence of suprathermal, fast electrons is observed. These pellets partly ablate before entering the plasma. This leads to a reduced penetration depth and to an additional fast gas pulse at the outside. One of the main advantages of pellet injection was found in experiments with NIH plasmas. By means of pellets the absorption for the neutral beams was increased without increasing the impurity content at the same time. This results in enhanced efficiency of the neutral beam heating and in reduced radiation losses for a given energy content compared with gas-fuelled discharges. In this way, an energy content of 4.8 kJ was achieved with pellets, which is above the energy contents achieved with gas puffing. However, the experiments reveal that the energy content of a discharge with a given density does not depend on the way of fuelling (pellet, gas puff). This is observed in OH, in ECRH as well as in NIH discharges.

As known from tokamaks the electron temperature profile recovers in about 2 ms to its pre-pellet shape. Reheating the plasma needs approximately the tenfold time, except in NIH plasmas. With NIH the reheating is faster, probably as a result of direct heating by fast ions.

The appearance of fluctuations in the emitted radiation during pellet ablation was very surprising. This effect, well known from tokamaks, was not expected in the nearly

shear-free stellarator. The current explanation of ablation fluctuations by rational flux surfaces is thus called in question and must presumably be revised. Also the experiments in W VII-A do not decide whether the fluctuations occur already during ablation or following ablation as a fast developing instability.

Acknowledgement

Technical support in developing and operating the pellet injector by J. Schiedeck, D. Köhler and J. Konrad is gratefully acknowledged. G. Weber is thanked for producing several figures.

References

[1] M. Kaufmann, Plasma Phys. **28** (9A), (1986)1341

[2] L.W. Jørgensen et al., Plasma Phys. **17** (1975), 453

[3] S. Sudo et al., Nucl. Fusion **25** (1985), 94

[4] W VII-A Team, NI Group, Proc. 9th Conf. Plasma Phys. and Contr. Nucl. Fusion, Baltimore 1-8 Sept.1982, Vol. II (1983) 241. Annual Reports IPP 1980, p. 23; 1981, p. 81; 1982, p. 66; 1983, p. 73; 1985 p. 104.

[5] K. Büchl et al., Proc.9th Symp.Eng.Probl.Fus.Res., Chicago 1981, Vol. II (1981), 1725.

[6] W VII-A Team, Proc.6th Conf.Plasma Phys.Contr.Nucl.Fusion, Berchtesgaden 6-13 Oct.1976, Vol. II (1977), 81.

[7] Annual Report IPP 1982, p. 36; 1983, p. 39.

Figure Captions

Fig. 1: Arrangement of the pellet injector in the W VII-A stellarator

Fig. 2: Particle content of pellets normalized to particle content of the W VII-A plasma for several pellet sizes.

Fig. 3: Vertical soft X-ray array in W VII-A.

Fig.4: Plasma current, ohmic power, line density and total energy content of pellet injection into OH plasma (#23293), $\iota(0) = 0.123, B(o) = 3.55T$, 1.0 mm ϕD_2 pellet, 500 m/s.

Fig. 5a: Arrangement to measure the H_α emission during pellet injection along the pellet direction.

Fig. 5b: Measured H_α during pellet ablation into OH plasma (#24389). Arrows indicate when the pellet entered and left the plasma.
1.0 mm ϕD_2 pellet.

Fig. 6: Measurement of SXR emission (2μBe) during pellet injection using a vertical XR array (Fig. 3). The records are not calibrated. The distance of the line of collimation from the axis on the torus diameter is given for each diode. 1.0 mm ϕD_2 pellet, 380 m/s, (#24227), OH plasma.
Pellet: dashed line; internal disruption: solid line.

Fig. 7: Electron temperature and density for several OH plasma shots at the torus axis before and after pellet injection, measured by single-point Thomson scattering diagnostics.

Fig. 8: Electron temperature profile before and after pellet injection into OH plasma, measured by ECE diagnostics (#24231).
1.0 mm ϕD_2 pellets.

Fig. 9: Total energy content of OH and ECRH plasmas without and with pellet injection, measured by a diamagnetic loop. Plasma current in OH plasmas: 20 kA and 30 kA. The density ranges from $0.5 \cdot 10^{13}\,\mathrm{cm}^{-3}$ to $5 \cdot 10^{13}\,\mathrm{cm}^{-3}$.

Fig. 10: Line density and total energy content (diamagnetic) of pellet injection into ECRH plasma ($\iota(0) = 0.51$)
RF: 70 GHz, 200 kW, $\Delta t = 60$msec (#63012). 0.6 mm ϕD_2 pellet, 570 m/s.

Fig. 11: Deposition profiles calculated for 0.6 mm ϕ (a) and 0.4 mm ϕ (b) pellets using the neutral gas shielding model for ECRH plasmas.

Fig. 12: Normalized electron temperature profiles measured by ECE diagnostics before and after pellet injection into ECRH plasma. $T_e(0)$ is decreased by a factor 0.4 by the pellet (#63033).
0.6 mm ϕD_2 pellets, 560 m/s.

Fig. 13: Variation of the total energy content of ECRH plasmas by pellet injection versus line density for several shots (#63024, 63027, 63029, 63030).
0.6 mm ϕD_2 pellet.

Fig. 14: Line density and total energy content (diameter) of pellet injection into ECRH plasma ($\iota(0) = 0.51$). RF = 70 GHz, 200 kW, Δt = 60 ms (#63003).

Fig. 15: Total radiated power for ECRH plasmas with pellet injection, measured by bolometry.
a) #63012; b) #63006.
0.6 mm ϕD_2 pellets, 570 m/s.

Fig.16: H_α emission during pellet injection measured by a diode (Fig. 1).
ECRH plasma: $\iota(0) = 0.60$ (#49252).
ECRH: 28 GHz, 150 kW.
0.8 mm ϕD_2 pellet, 530 m/s.

Fig. 17: Pellet ablation trace in NIH plasma with traces of sputtered particles. For explanation see Fig. 27 (#57109).
0.8 mm ϕD_2 pellet, 600 m/s.

Fig. 18: Electron temperature and density at the torus axis before and after pellet injection for several NIH discharges, measured by single-point Thomson scattering diagnostics (#27024 – 27041).
1.0 mm ϕD_2 pellets.

Fig. 19: Line density, electron temperature (XR) and total energy content of NIH plasmas with pellet injection, OH target plasma.
NIH : 1.7 MW, $\iota(0) = 0.165, B_t = 3.5T$.
a) #36950; b) #36946.
0.6 mm ϕD_2 pellets, 610 m/s.

Fig. 20: Variation of total energy content of NIH plasma versus line density: #34420 without pellet, #34469 with pellet.

0.6 mm ϕD_2 pellet.

Fig. 21: Line density of NIH discharges with different rotational transforms $\iota(a)$ and with and without pellet injection.
0.6 mm ϕD_2 pellets.
a) $\iota(a) = 0.45$ (non-rational); #34469 with pellet, #34420 without pellet.
b) $\iota(a) = \frac{1}{3}$ (rational); #38990 with pellet, #38988 without pellet.

Fig. 22: Line density, electron temperature (XR) and total energy content of NIH plasmas with pellet injection, ECRH target plasma.
NIH : 1.3 MW, $\iota(0) = 0.45$, $B_t = 2.6T$.
a) #62262; b) #62274.
0.6 mm ϕD_2 pellets, 590 m/s.

Fig. 23: SXR emission ($0.0\mu Be$) during pellet injection, measured by the vertical XR array in the injection plane. The distance of the line of collimation on a diameter is given for each diode.
(#37986), NIH plasma.
0.6 mm ϕD_2 pellets.

Fig. 24: XR emission profiles at various times during pellet injection. Signals relative to pre-pellet level. Negative scale enlarged, (#37986).
0.6 mm ϕD_2 pellets, 590 m/s.

Fig. 25: Line density and total energy content for simultaneous NIH and ECRH plasma with pellet injection.
NIH: 1.3 MW, ECRH: 200 kW at 28 GHz, $\iota(0) = 0.60, B_t = -1.0\ T$, #49256.
0.8 mm ϕD_2 pellets.

Fig. 26: H_α emission during pellet injection into simultaneous NIH and ECRH plasma.
NIH: 1.3 MW, ECRH: 200 kW at 28 GHz, #49242.
0.8 mm ϕD_2 pellets.

Fig. 27: Description of photos in Figs. 17 and 28 – 30. Top view of radial ablation trace.

Fig. 28: Photographs of ablation traces in ECRH plasmas. Top view of radially injected pellets.
ECRH: 200 kW at 70 GHz, $\iota(0) = 0.5 \ldots 0.6$.
0.6 mm ϕD_2 pellets, 580 m/s.
a) #63015, b) #63042, c) #63040, d) #63005.

Fig. 29: Photograph of ablation trace in NIH plasma (top view).
NIH: 1.3 MW, $\iota(0) = 0.45$, #57112.
0.8 mm ϕD_2 pellets, 640 m/s.

Fig. 30: Photograph of ablation trace of a splitting pellet in OH plasma (top view)
#54446.
0.8 mm ϕD_2 pellets.

Table 1 Pellet Injection in W VII A

		OH	ECRH	N I H OH-Target	N I H ECRH-Target	ECRH + NIH
Plasma density $\bar{n}$	$[cm^{-3}]$	$0.5\text{-}5.0\cdot10^{13}$	$0.5\text{-}1.5\cdot10^{13}$	$2\text{-}3\cdot10^{13}$	$2.5\cdot10^{13}$	$0.5\cdot10^{13}$
Pellet	Ø [mm]	1.0	0.6	0.6 (0.8)	0.6	0.8
	N_{Pel}/N_{Pla} [%]	200 - 1000	400	100	100	~1000
Deposition	$\Delta\bar{n}$ $[cm^{-3}]$	$1\text{-}5\cdot10^{13}$	$0.7\cdot10^{13}$	$1.5\cdot10^{13}$	$1.5\cdot10^{13}$	$0.6\cdot10^{13}$
	N_{dep}	$0.8\text{-}2\cdot10^{19}$	$2.6\cdot10^{18}$	$8\cdot10^{18}$ ($8\text{-}10\cdot10^{18}$)	$8\cdot10^{18}$	$\sim 3\cdot10^{18}$
	N_{dep}/N_{pel} [%]	25 - 50 %	30 %	100 % (30-50 %)	100 %	5 - 10 %
Penetration	d_{Pel} [cm]	> 20	10	> 20 (1.0 mmØ)	[6 - 8]	5
	time of flight [µs]	> 400	-	> 400	-	> 400
Ablation	ΔE [J]	200-400	5 - 60	20 - 50 [200]	< 50	< 50
Temperature	ΔT_e [eV]	350	350	120 - 270	150-300	-
	$\Delta t_{Profile}$ [ms]	4	2 - 3	-	-	-
	Δt_{Reheat} [ms]	15 - 20	10	~2	-	-
Density	Δt_{Decay} [ms]	> 100	> 100	30 ms, > 100	> 100	< 10 ms
Plasma Energy	max. content [J]	1400	400	4800	2000	-
	E	increase, decrease	increase	increase	increase	decrease

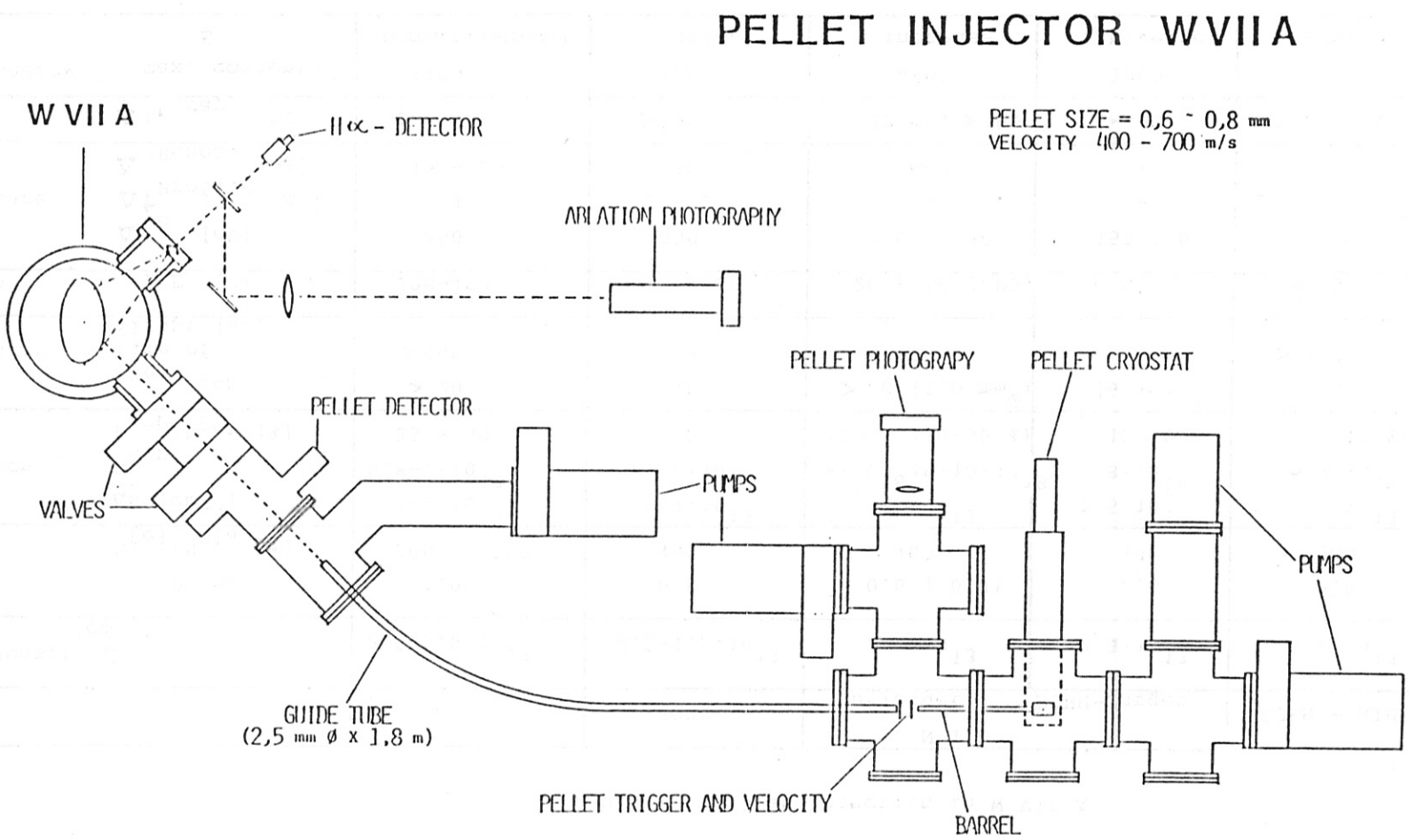
PELLET INJECTOR WVII A
W VII A
Hα - DETECTOR
PELLET SIZE = 0,6 ~ 0,8 mm
VELOCITY 400 - 700 m/s
ABLATION PHOTOGRAPHY
PELLET PHOTOGRAPY
PELLET CRYOSTAT
PELLET DETECTOR
PUMPS
VALVES
PUMPS
GUIDE TUBE
(2,5 mm Ø x 1,8 m)
PELLET TRIGGER AND VELOCITY
BARREL

Figure 1

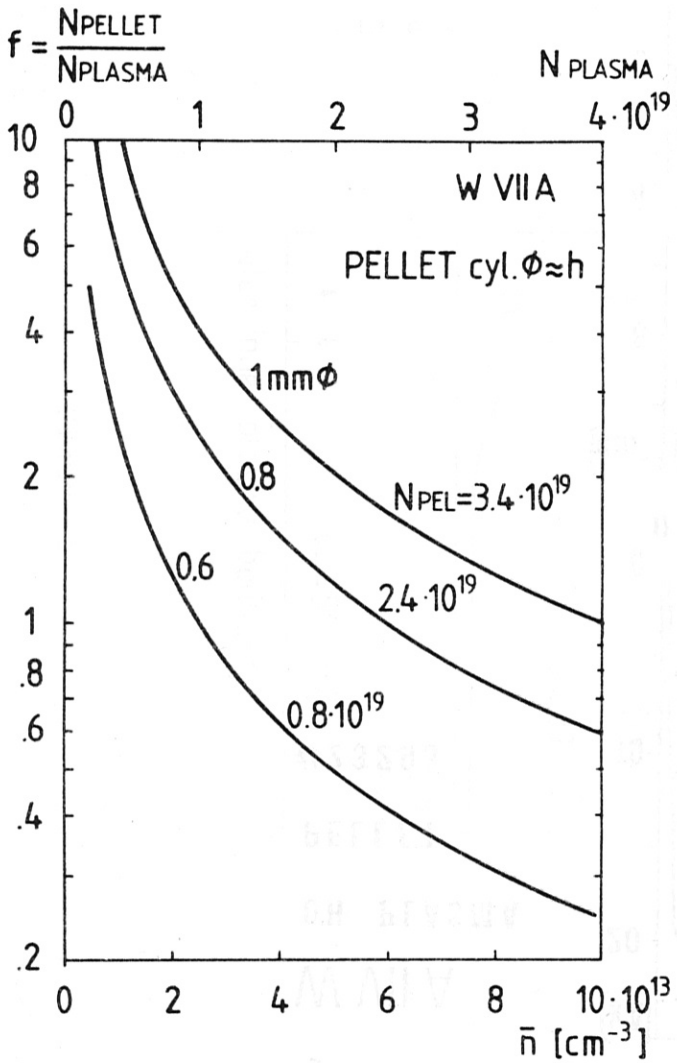

Figure 2

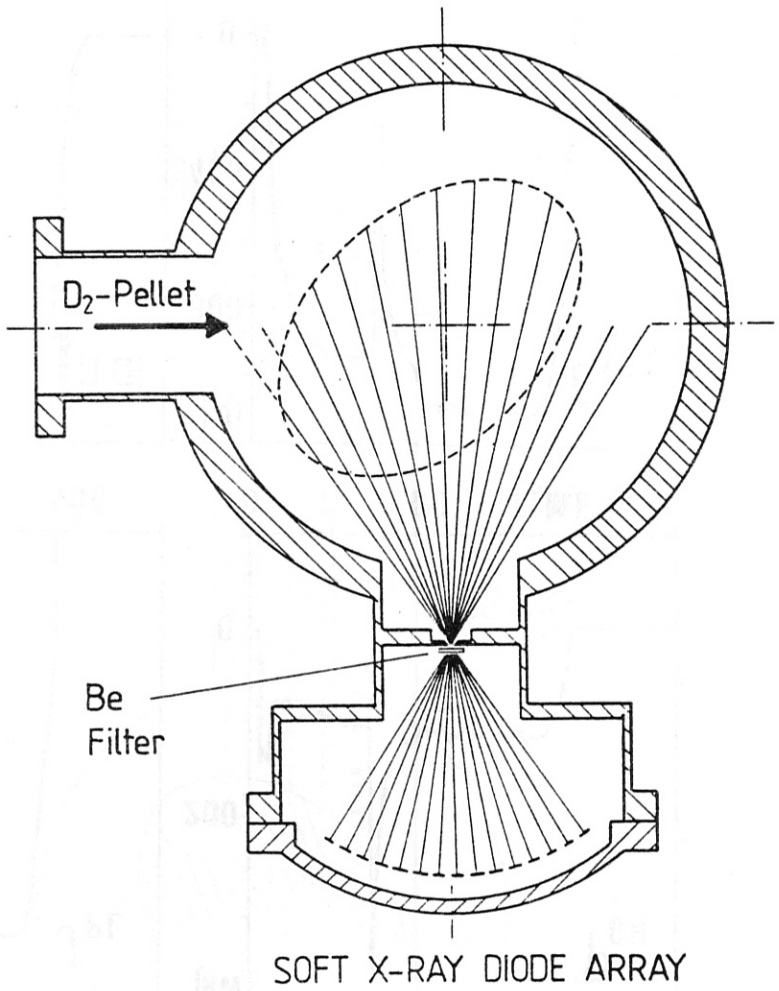

Figure 3

W VII A

OH PLASMA

PELLET

#23293

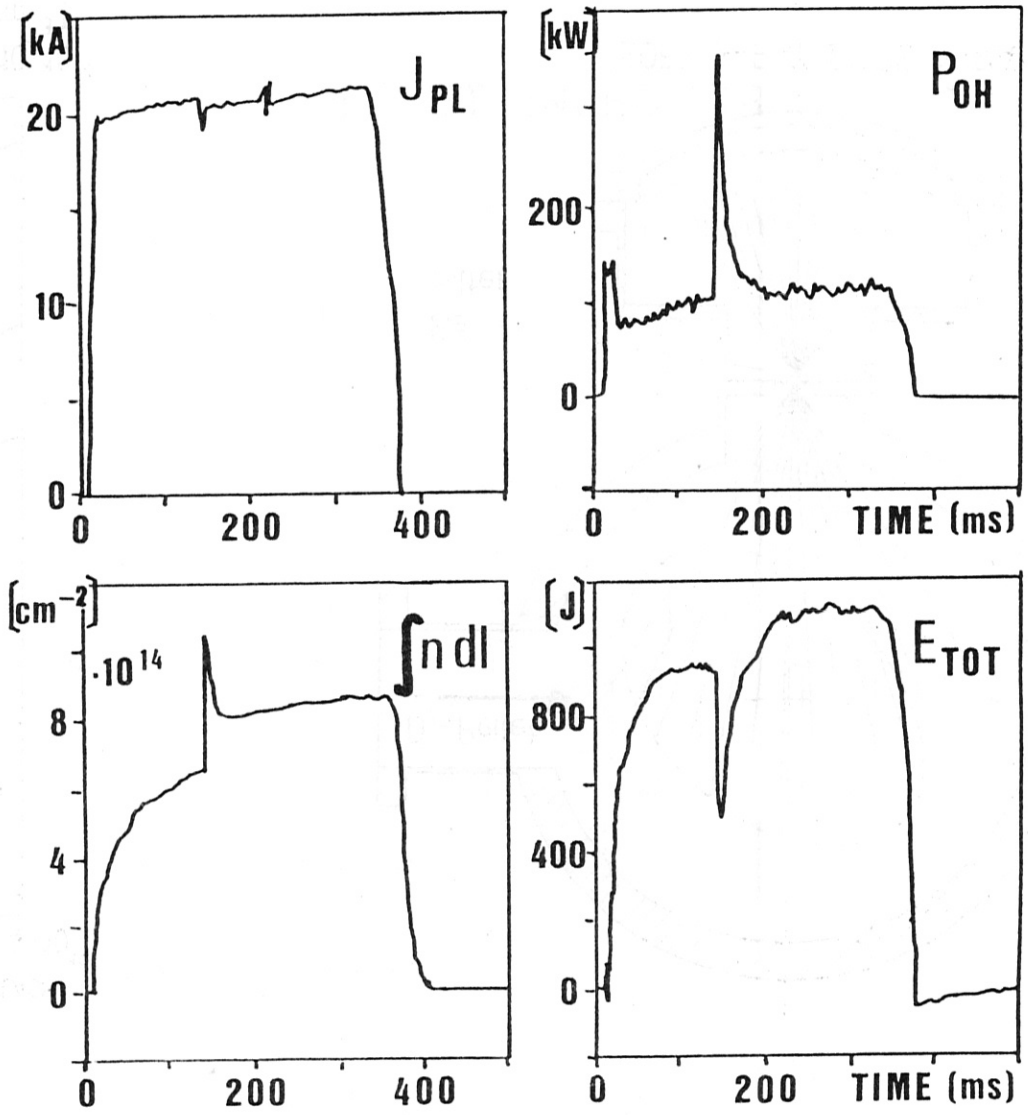

Figure 4

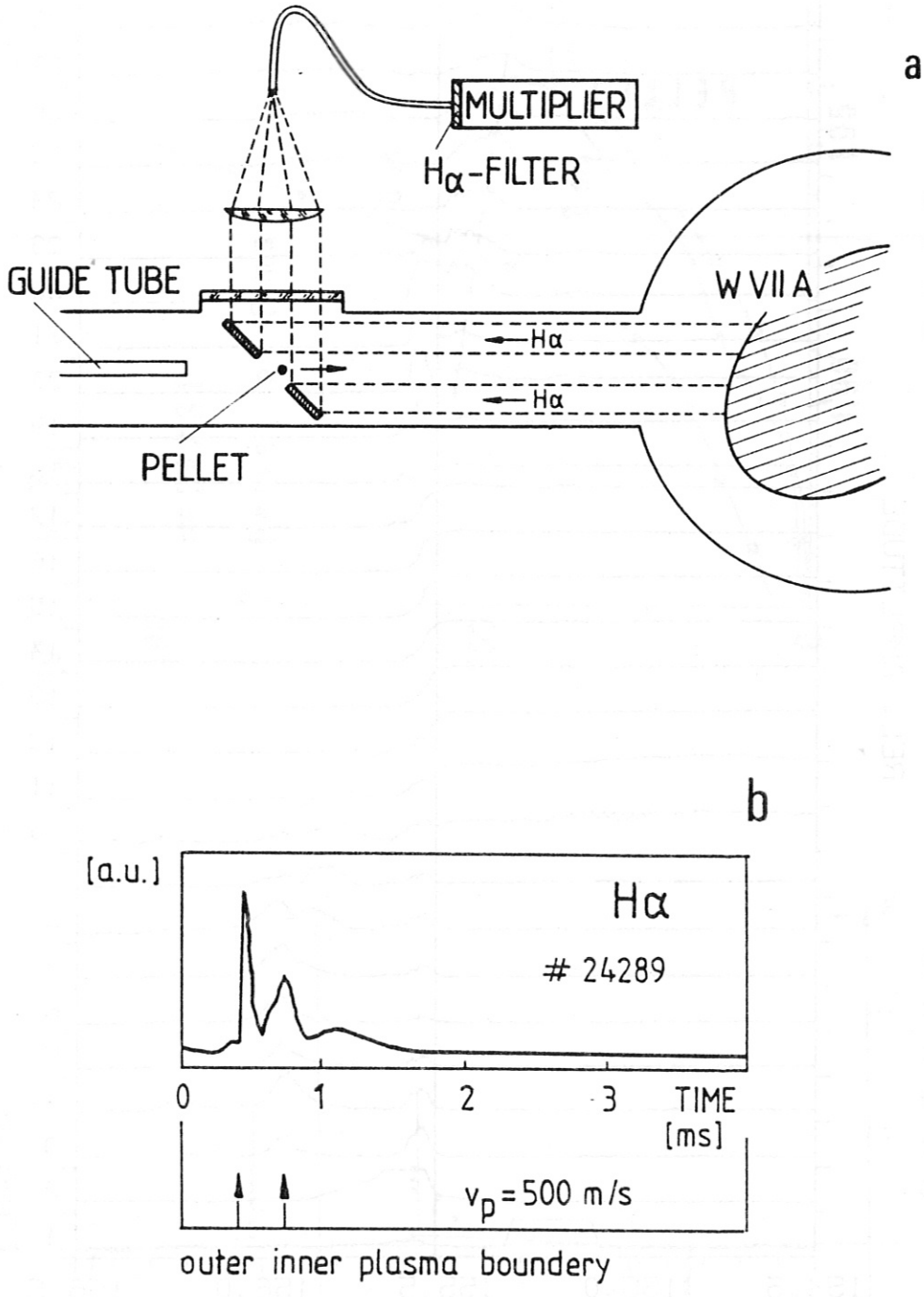
a
MULTIPLIER
Hα-FILTER
GUIDE TUBE
W VII A
Hα
Hα
PELLET
b
[a.u.]
Hα
24289
0
1
2
3
TIME
[ms]
v_p = 500 m/s
outer inner plasma boundery

Figure 5

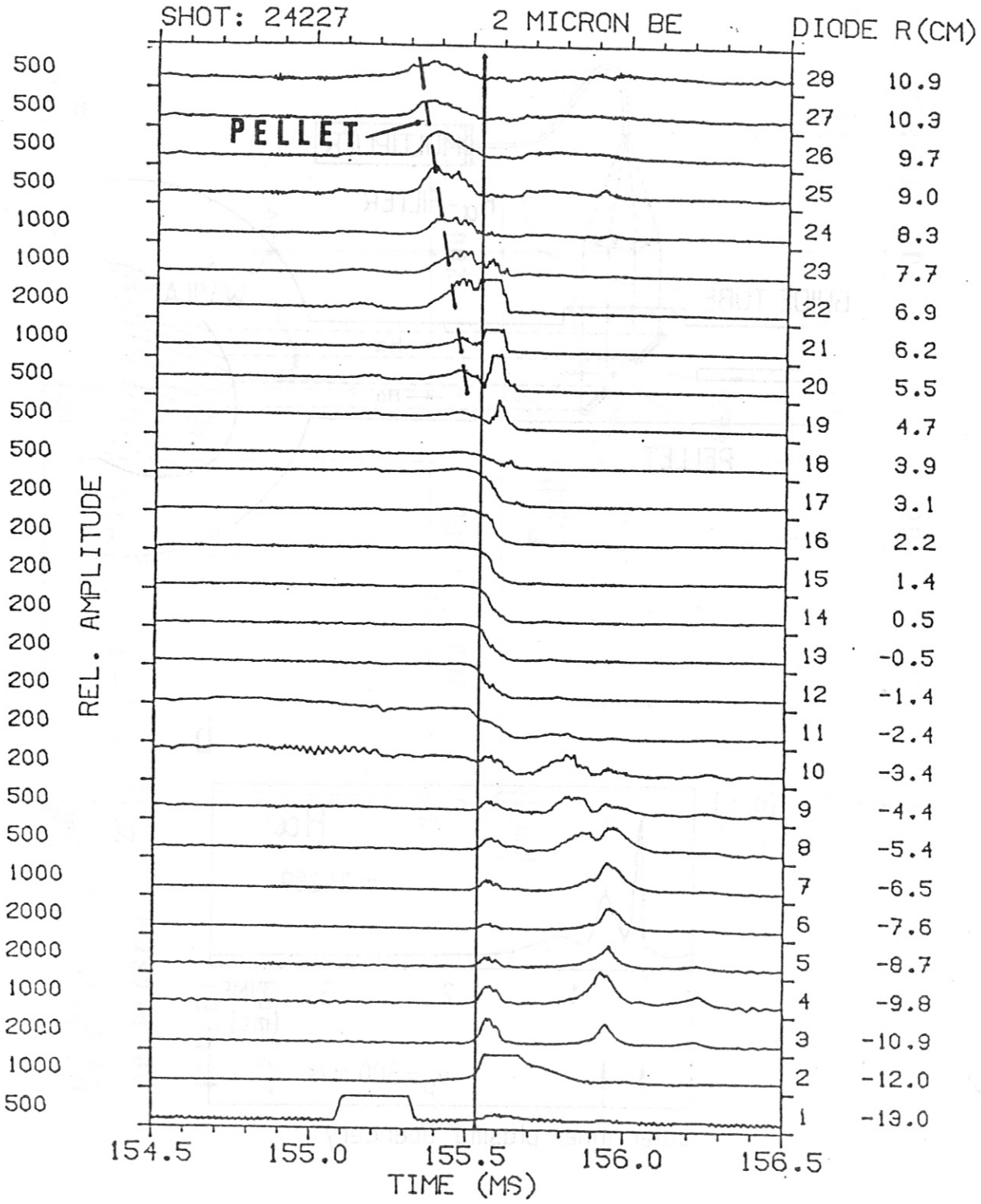
SHOT: 24227
2 MICRON BE
DIODE R(CM)
PELLET
REL. AMPLITUDE
TIME (MS)
154.5
155.0
155.5
156.0
156.5
28 10.9
27 10.3
26 9.7
25 9.0
24 8.3
23 7.7
22 6.9
21 6.2
20 5.5
19 4.7
18 3.9
17 3.1
16 2.2
15 1.4
14 0.5
13 -0.5
12 -1.4
11 -2.4
10 -3.4
9 -4.4
8 -5.4
7 -6.5
6 -7.6
5 -8.7
4 -9.8
3 -10.9
2 -12.0
1 -13.0

Figure 6

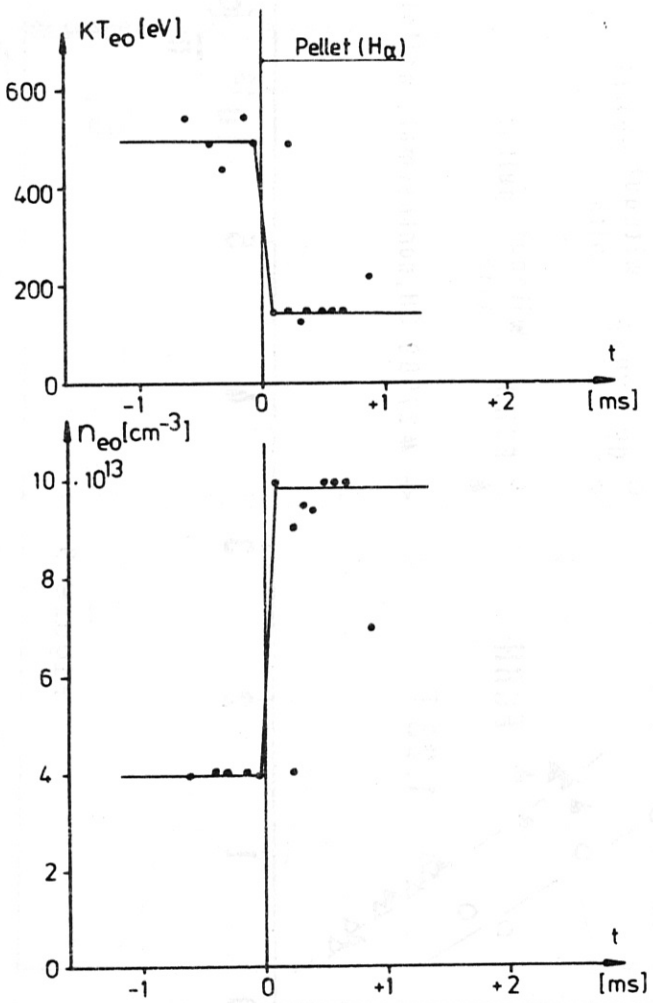

Figure 7

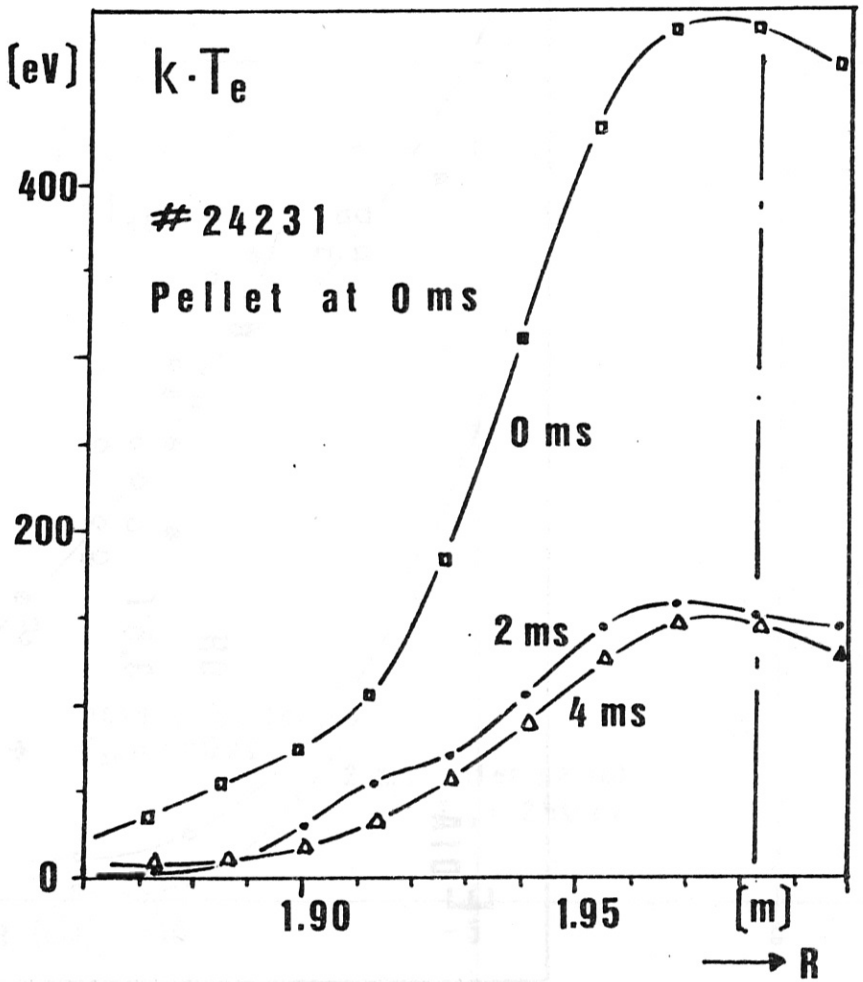

Figure 8

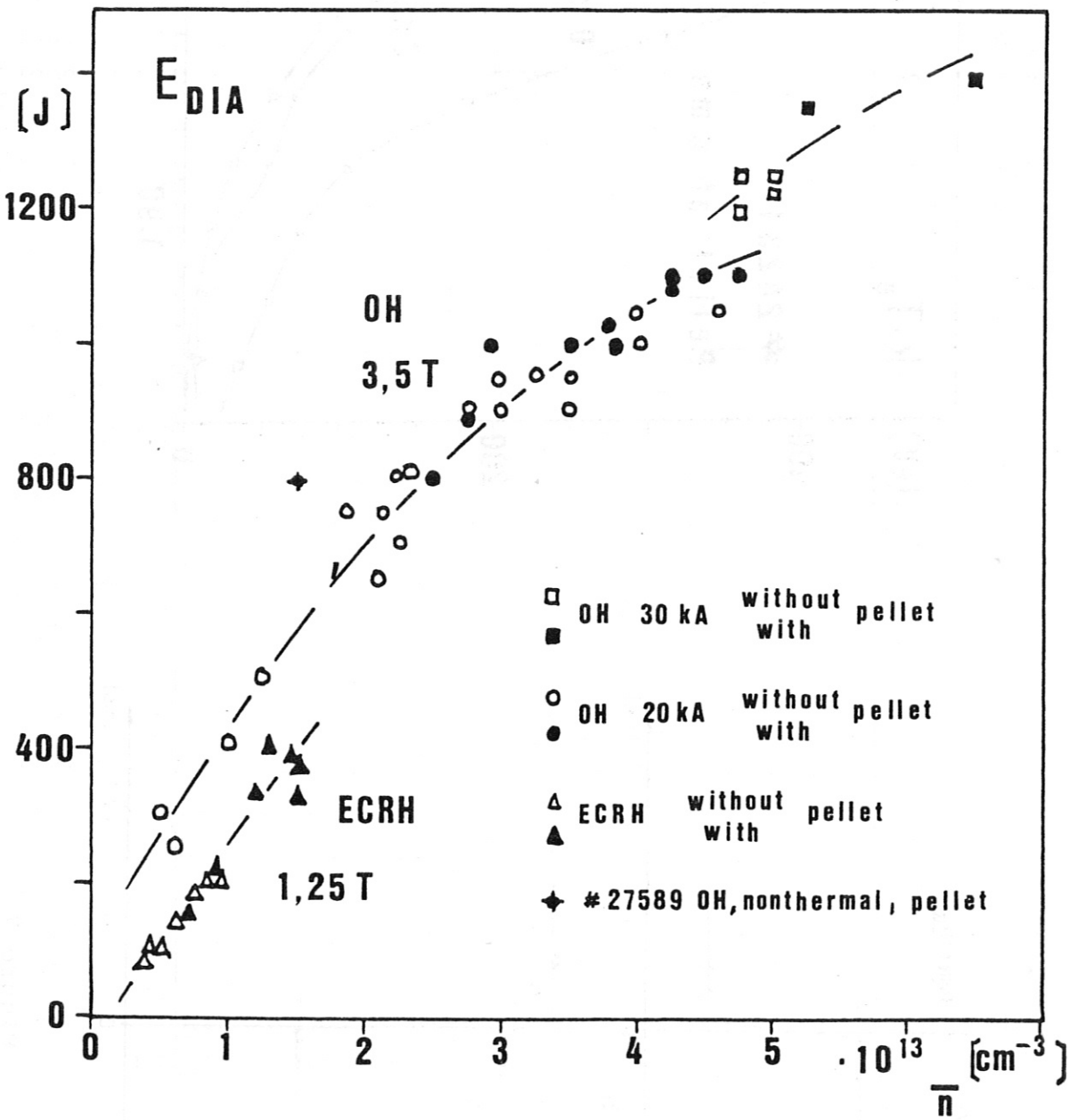
E DIA
[J]
1200
800
400
0
OH
3,5 T
ECRH
1,25 T
OH 30 kA without pellet
with
OH 20 kA without pellet
with
ECRH without pellet
with
27589 OH, nonthermal, pellet
0
1
2
3
4
5
·10 13 [cm-3]
n

Figure 9

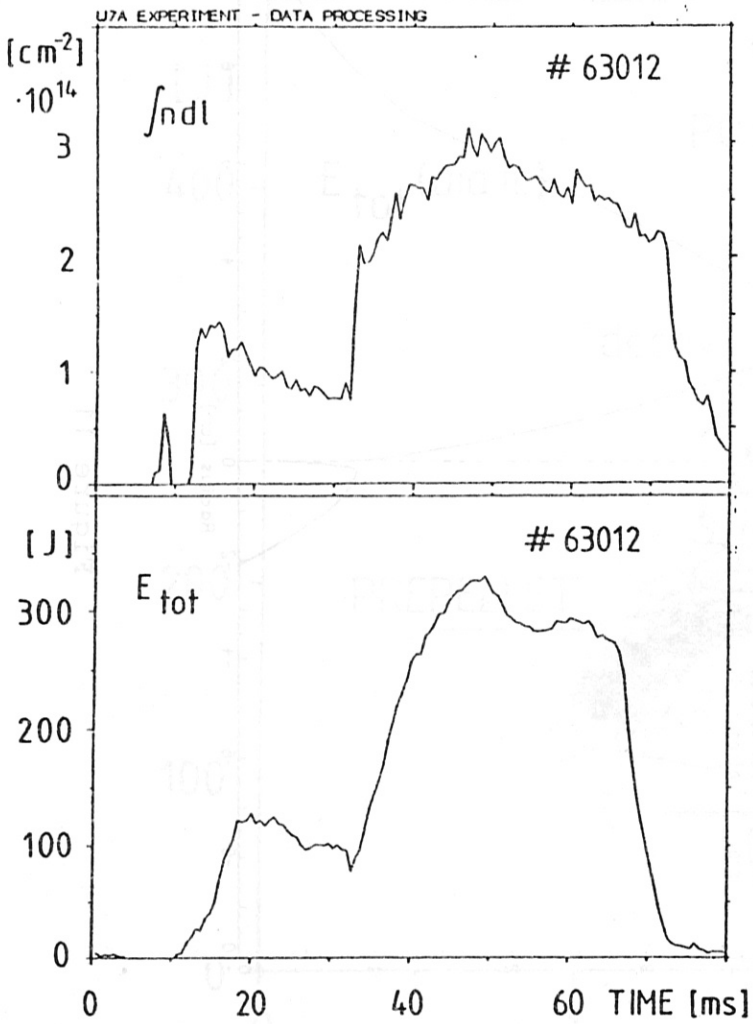

Figure 10

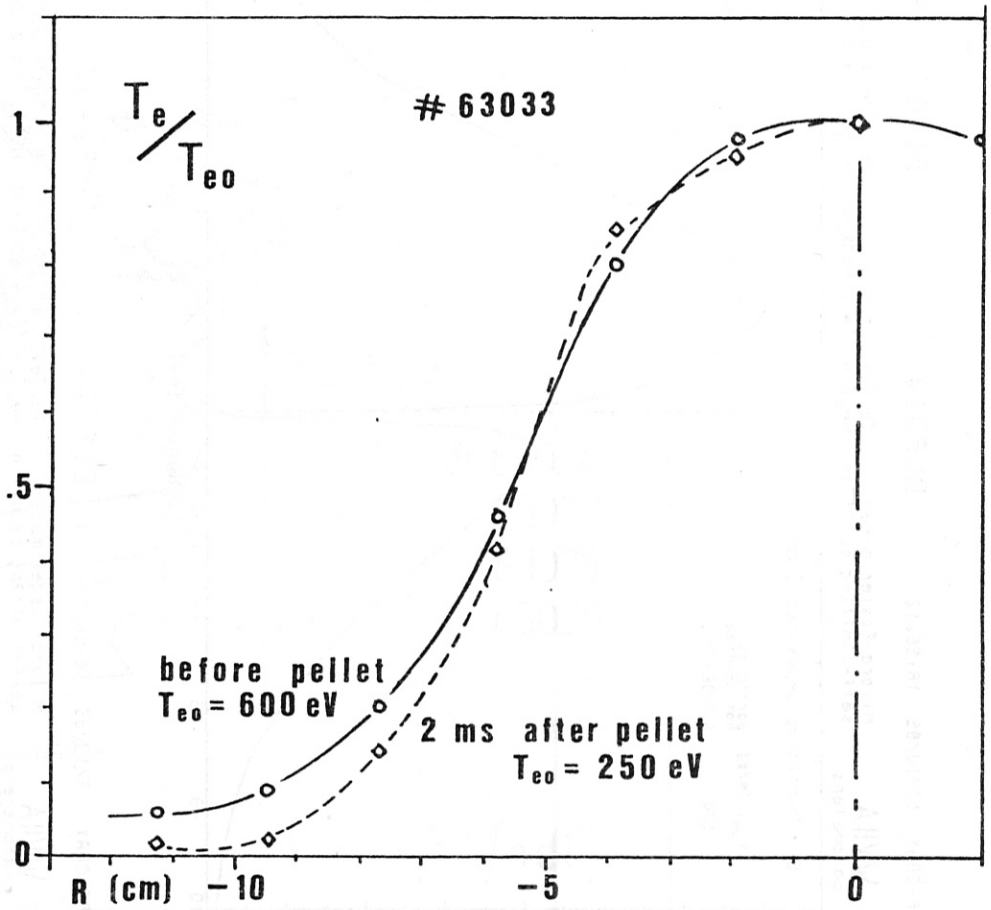

Figure 12

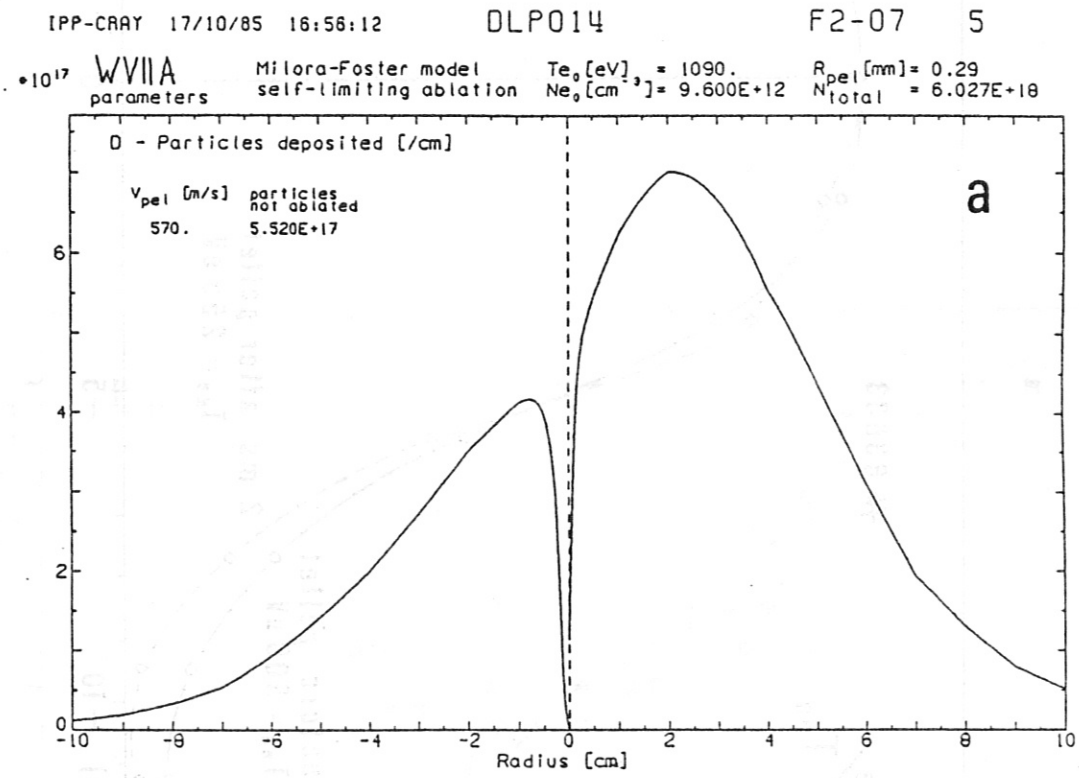
IPP-CRAY 17/10/85 16:56:12 DLP014 F2-07 5
•10^17 WVIIA parameters
Milora-Foster model self-limiting ablation
Te0[eV] = 1090. Ne0[cm^-3]= 9.600E+12
Rpel[mm]= 0.29 Ntotal = 6.027E+18
D - Particles deposited [/cm]
Vpel [m/s] particles not ablated
570. 5.520E+17
a
Radius [cm]

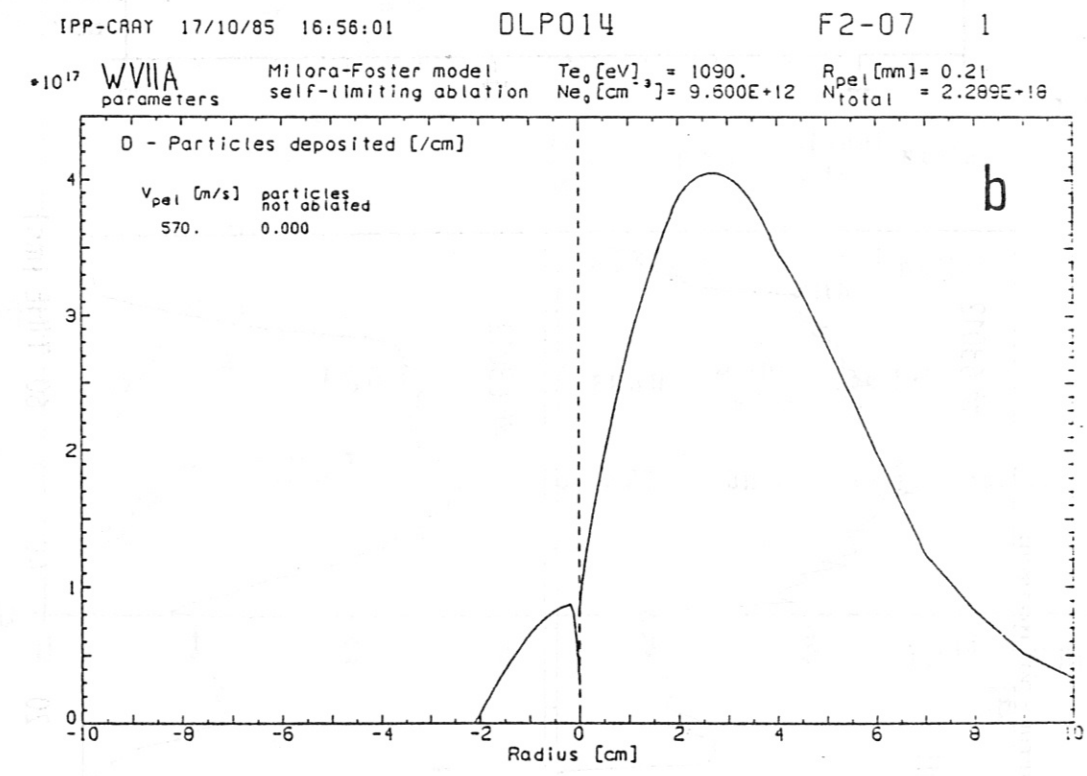
IPP-CRAY 17/10/85 16:56:01 DLP014 F2-07 1
•10^17 WVIIA parameters
Milora-Foster model self-limiting ablation
Te0[eV] = 1090. Ne0[cm^-3]= 9.600E+12
Rpel[mm]= 0.21 Ntotal = 2.289E+18
D - Particles deposited [/cm]
Vpel [m/s] particles not ablated
570. 0.000
b
Radius [cm]

Figure 11

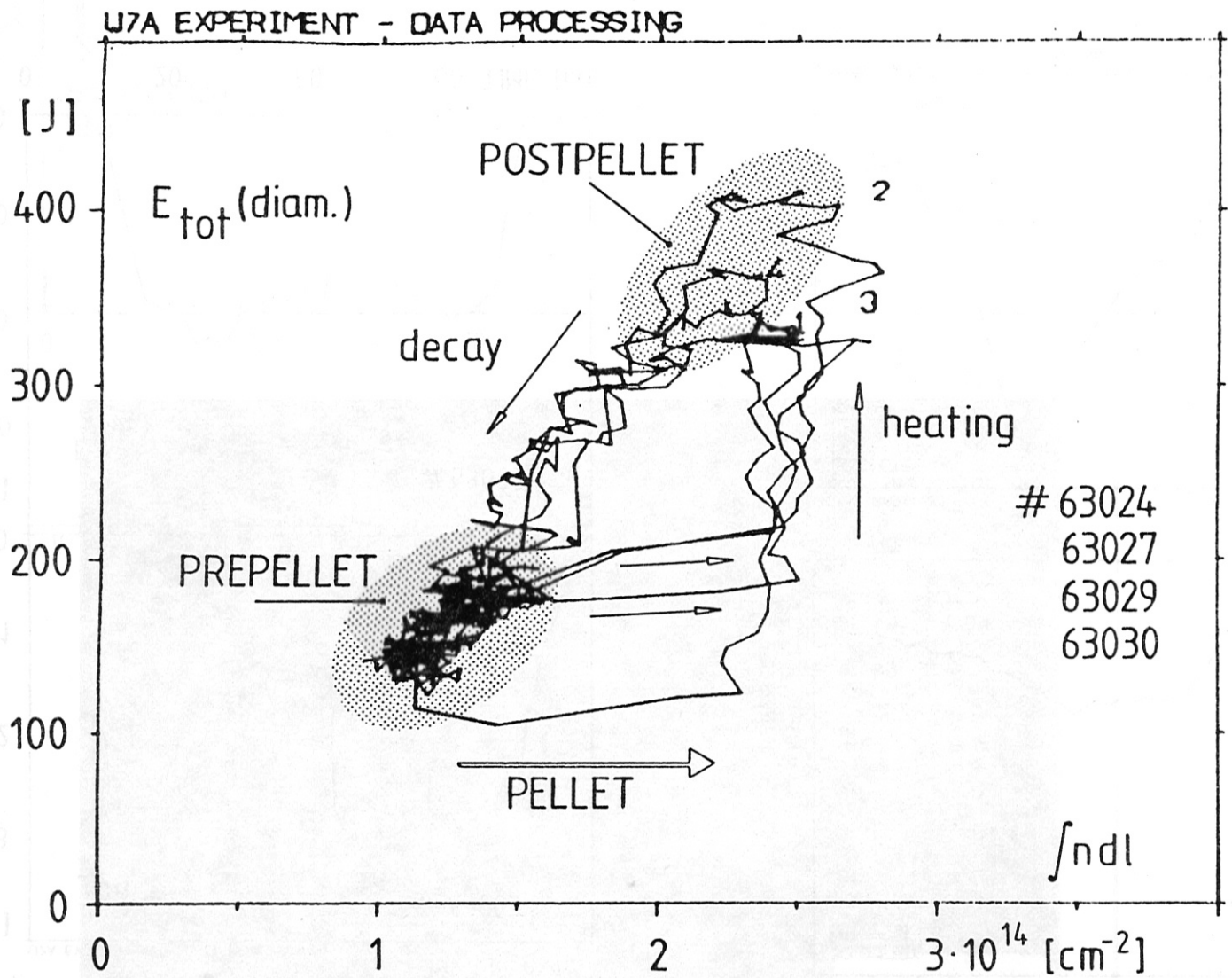
UJ7A EXPERIMENT - DATA PROCESSING
[J]
400
300
200
100
0
E_{tot} (diam.)
POSTPELLET
2
3
decay
heating
PREPELLET
63024
63027
63029
63030
PELLET
∫ndl
0
1
2
$3 \cdot 10^{14}$ [cm^{-2}]

Figure 13

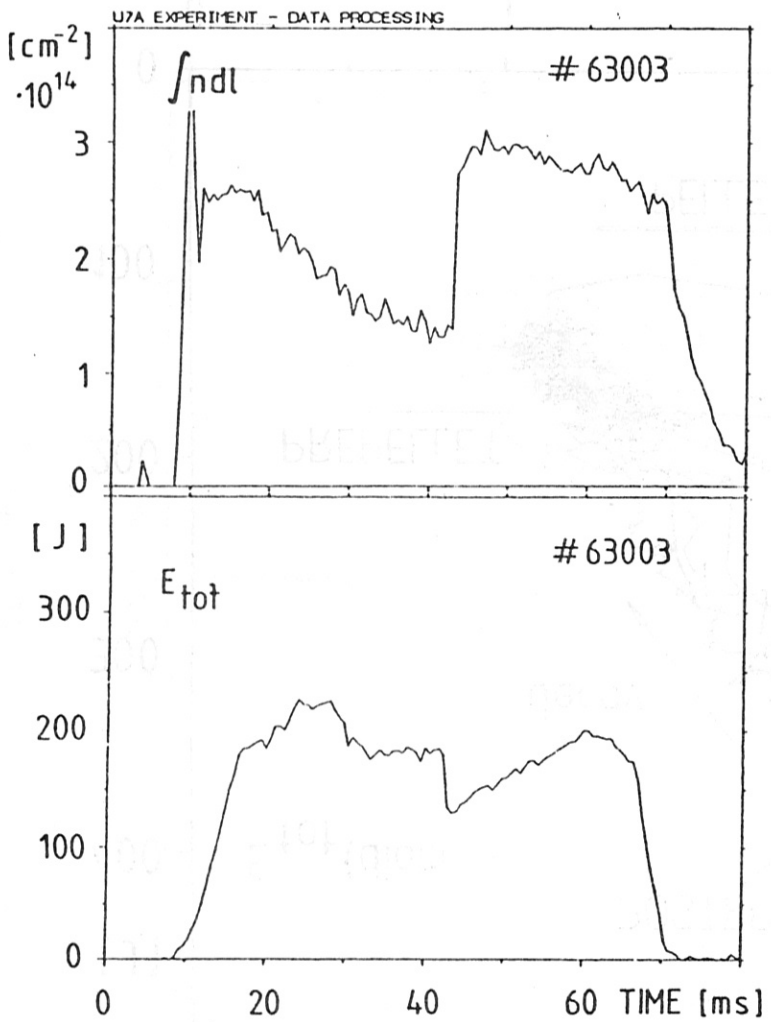

Figure 14

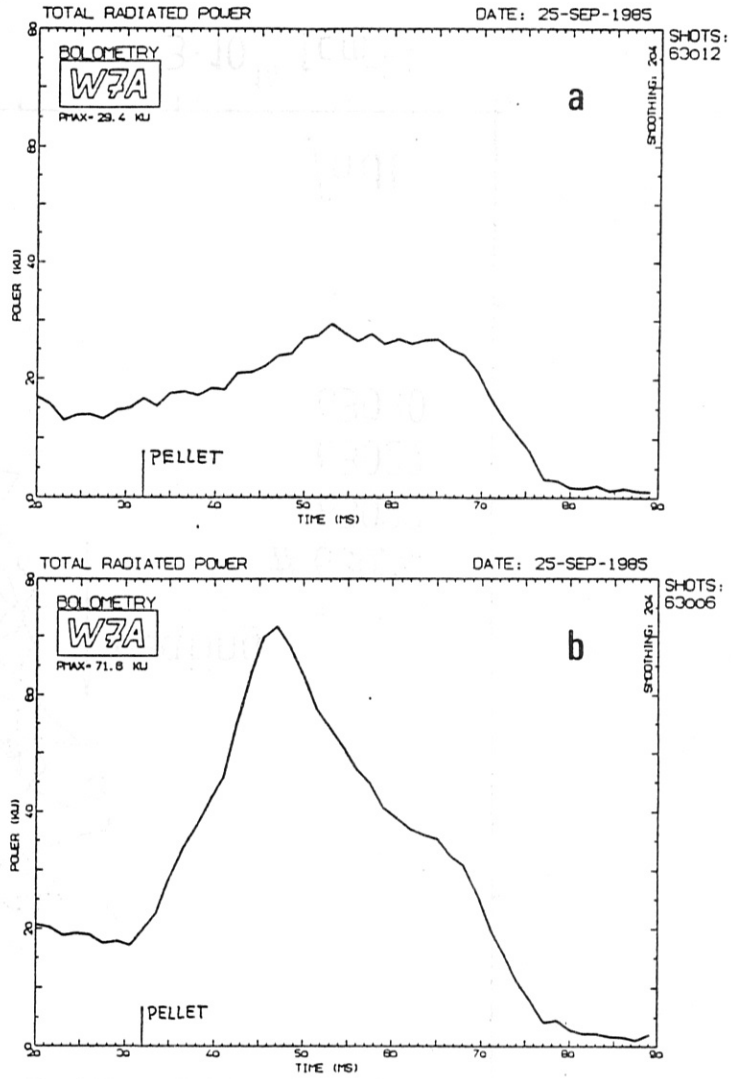

Figure 15

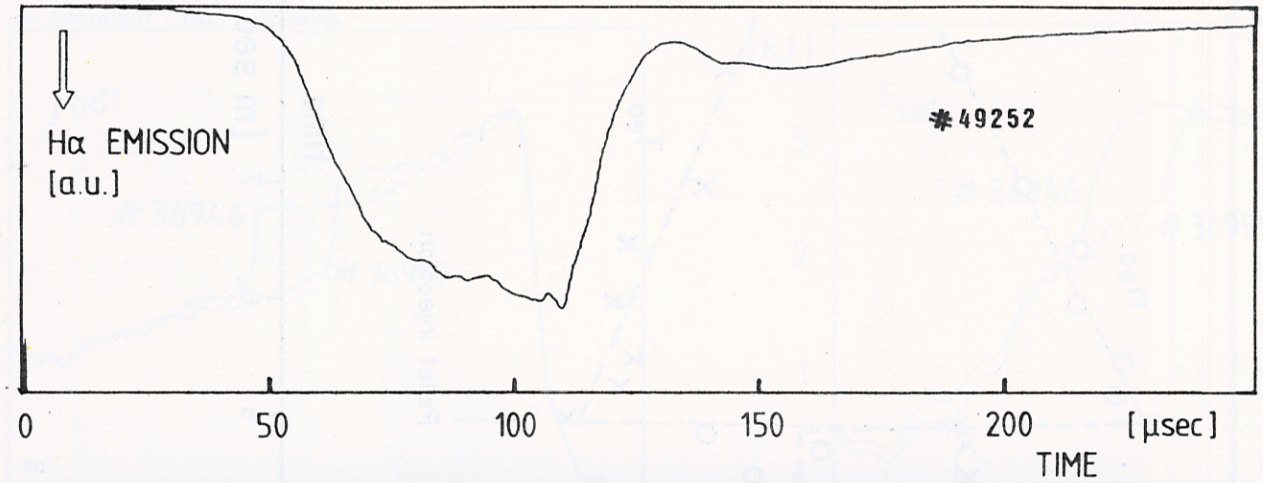

Figure 16

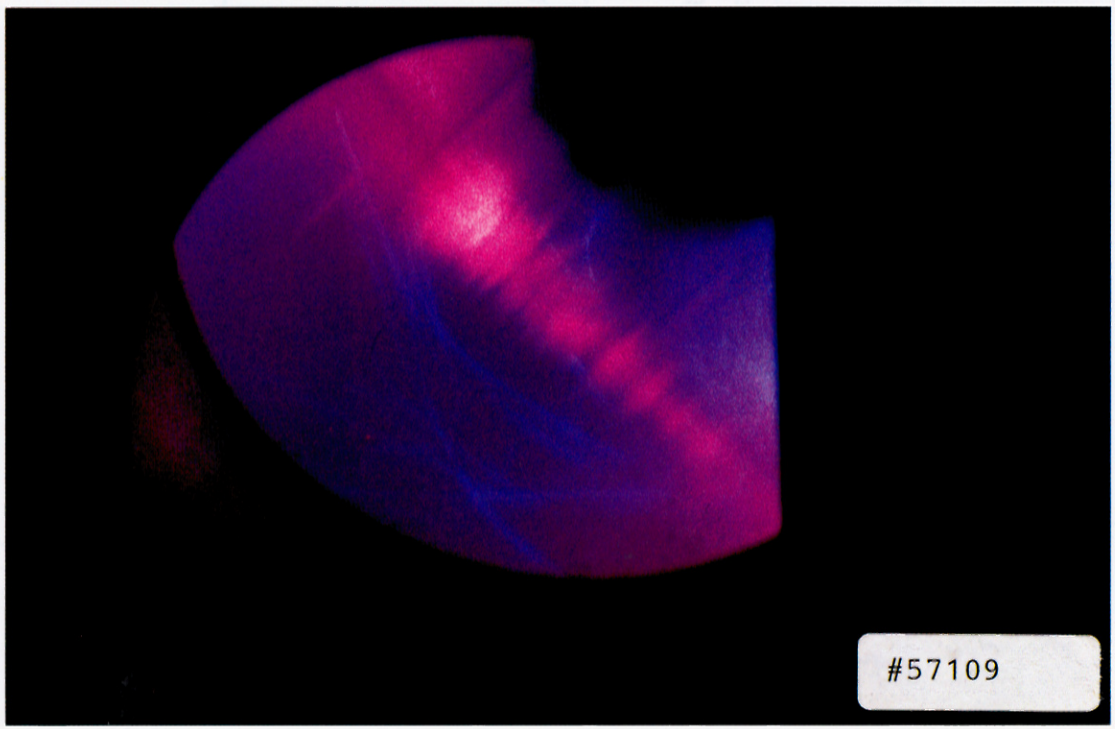

Figure 17

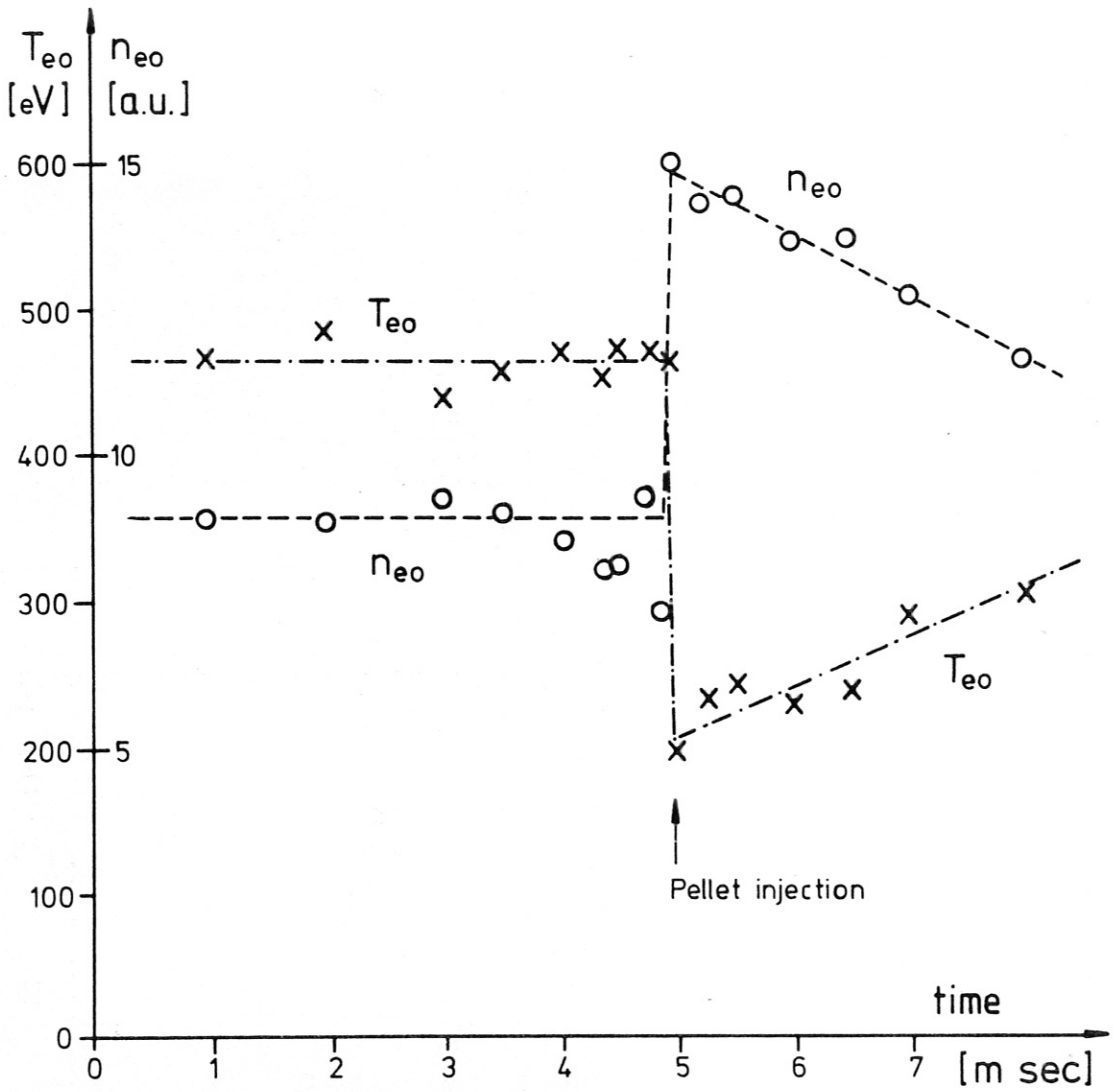
T_{eo} [eV]
n_{eo} [a.u.]
600
500
400
300
200
100
0
15
10
5
T_{eo}
n_{eo}
n_{eo}
T_{eo}
Pellet injection
time
0
1
2
3
4
5
6
7
[m sec]

Figure 18

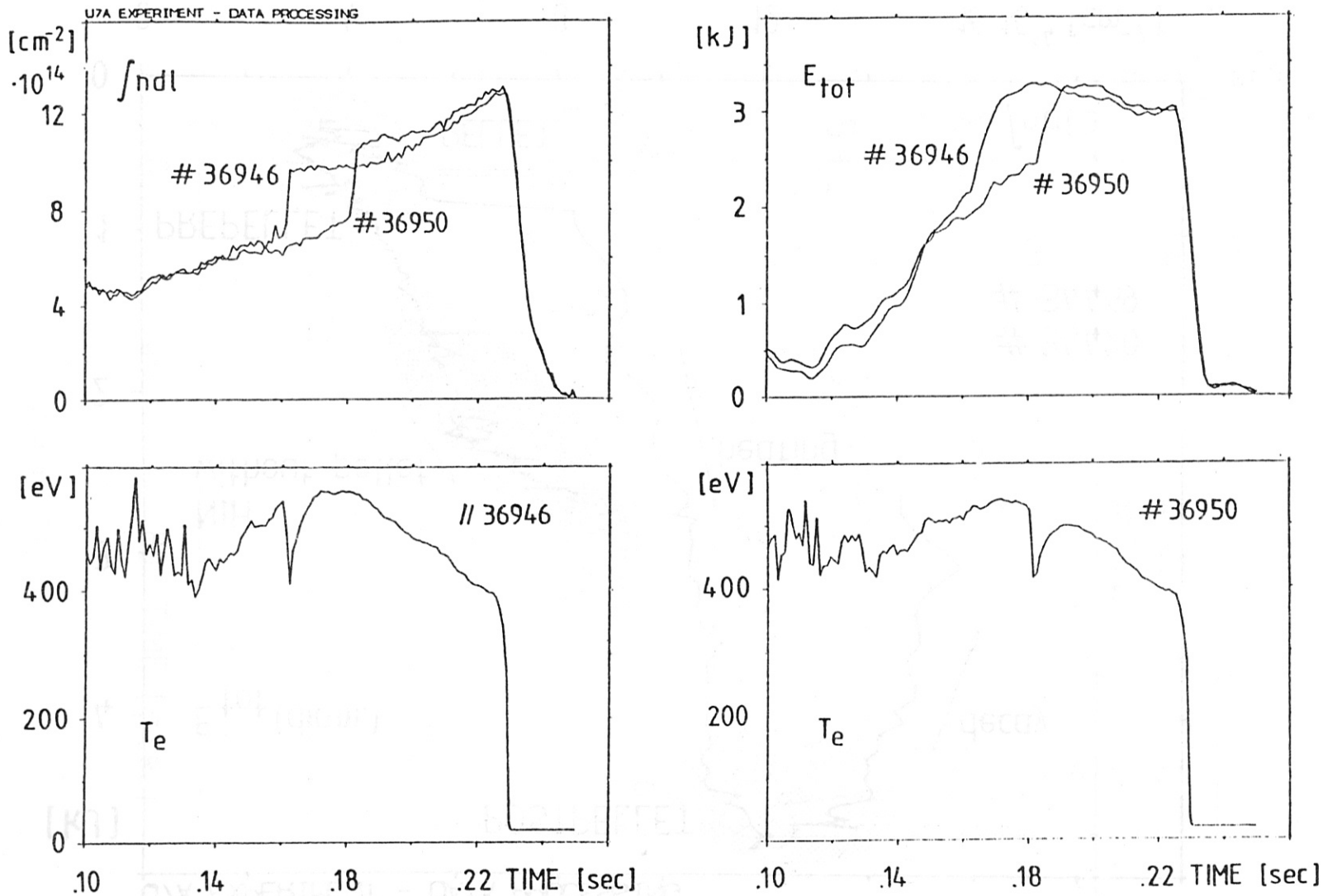
U7A EXPERIMENT - DATA PROCESSING
[cm⁻²]
·10¹⁴
12
8
4
0
∫ndl
36946
36950
[kJ]
3
2
1
0
E tot
36946
36950
[eV]
400
200
0
Te
// 36946
36950
.10
.14
.18
.22 TIME [sec]

Figure 19

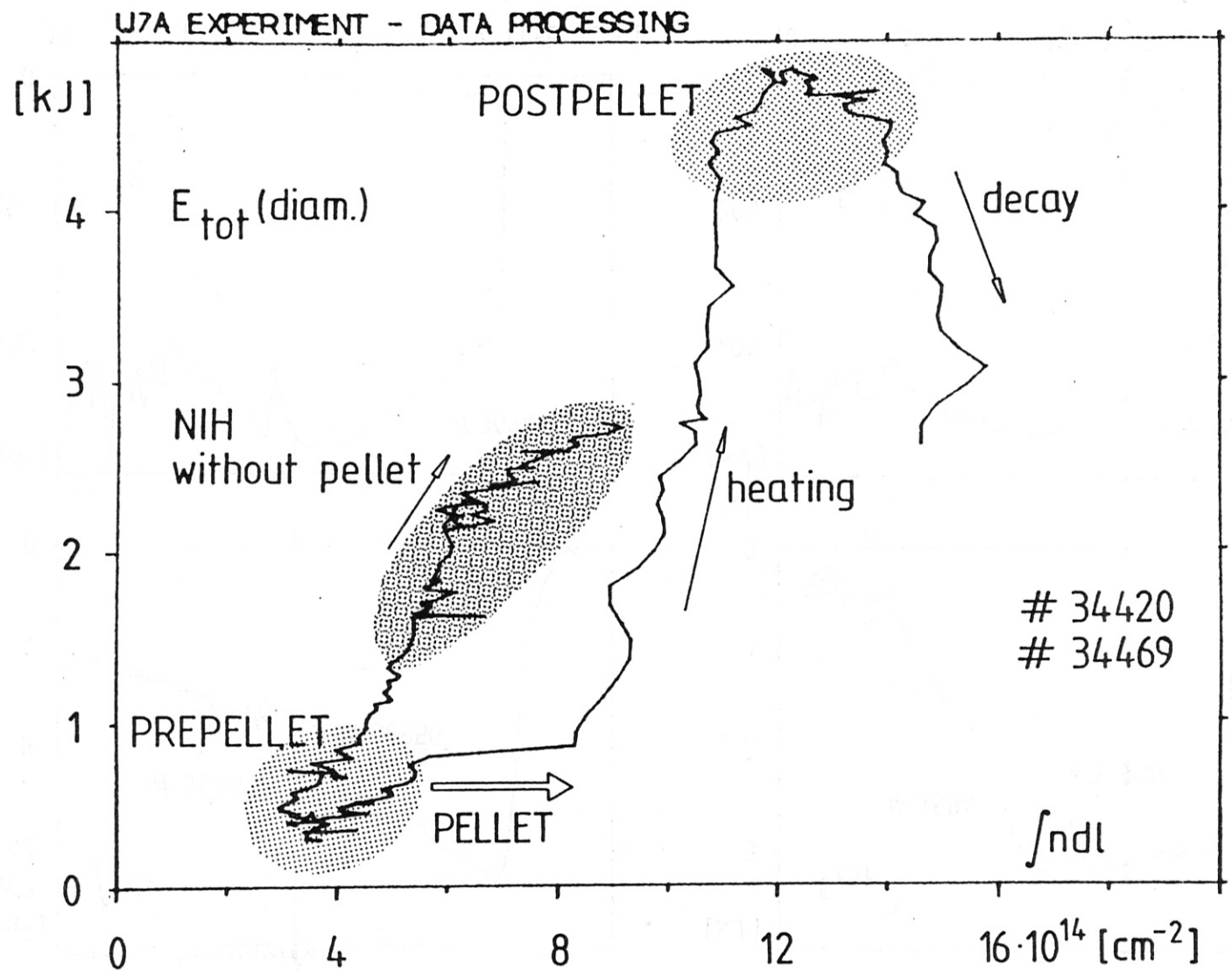
U7A EXPERIMENT - DATA PROCESSING
[kJ]
POSTPELLET
E_{tot} (diam.)
decay
NIH
without pellet
heating
34420
34469
PREPELLET
PELLET
∫ndl
0
1
2
3
4
0
4
8
12
$16 \cdot 10^{14}$ [cm^{-2}]

Figure 20

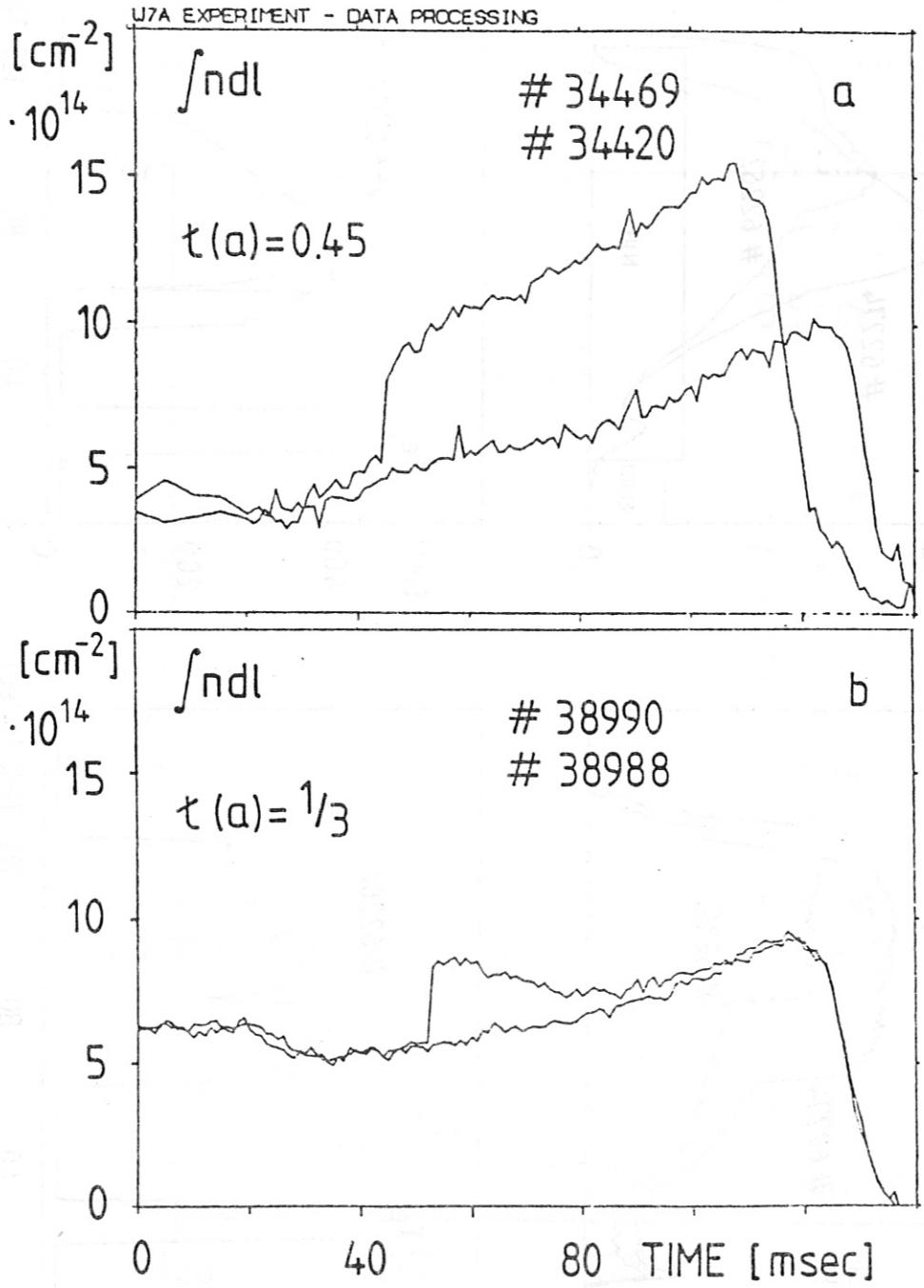
U7A EXPERIMENT - DATA PROCESSING
[cm⁻²]
·10¹⁴
∫ndl
34469
34420
a
t(a)=0.45
15
10
5
0
[cm⁻²]
·10¹⁴
∫ndl
38990
38988
b
t(a)= 1/3
15
10
5
0
0
40
80 TIME [msec]

Figure 21

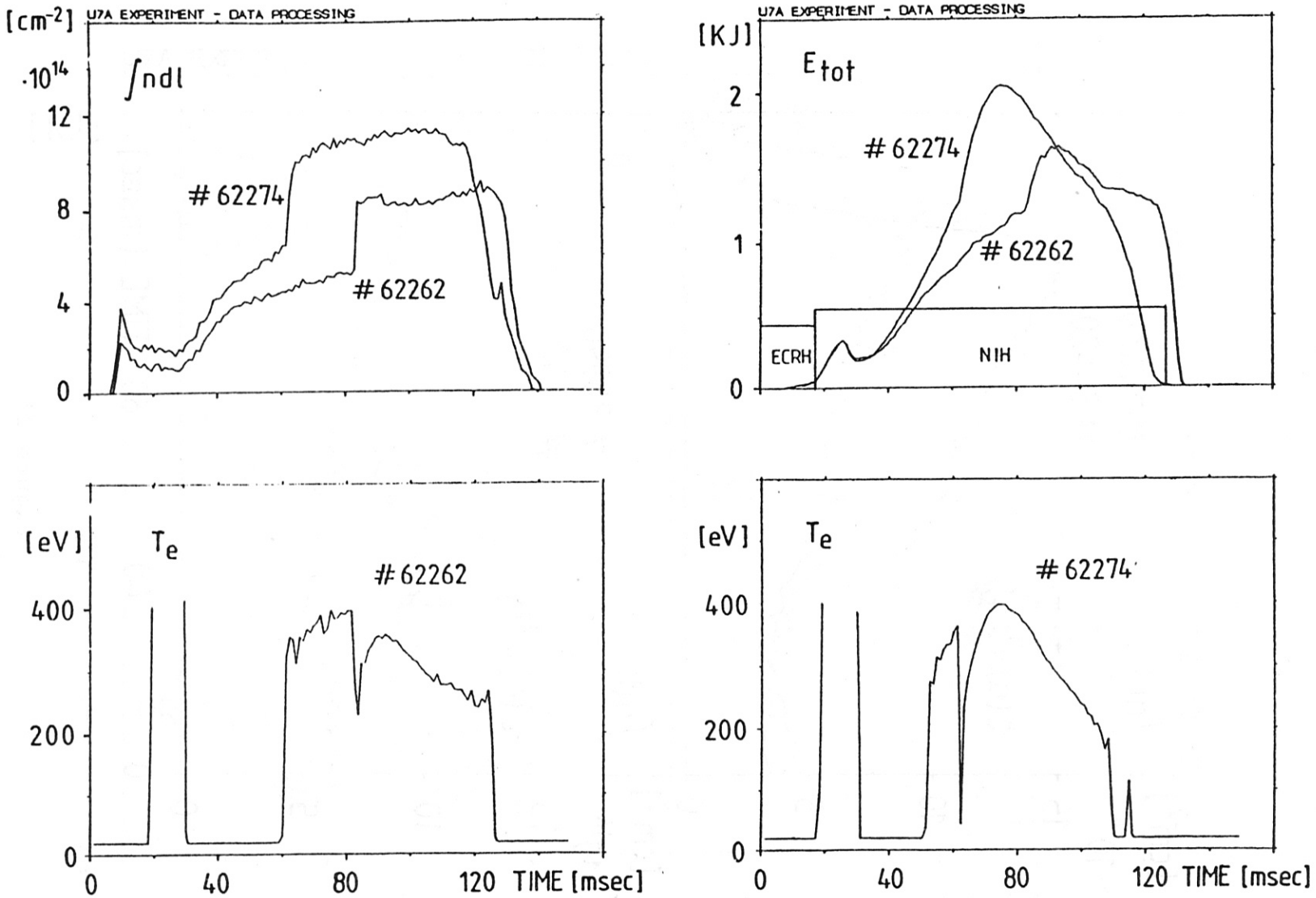
U7A EXPERIMENT - DATA PROCESSING
[cm-2]
·10^14
∫ndl
12
8
4
0
62274
62262
U7A EXPERIMENT - DATA PROCESSING
[KJ]
Etot
2
1
0
62274
62262
ECRH
NIH
[eV]
Te
400
200
0
62262
0
40
80
120 TIME [msec]
[eV]
Te
400
200
0
62274
0
40
80
120 TIME [msec]

Figure 22

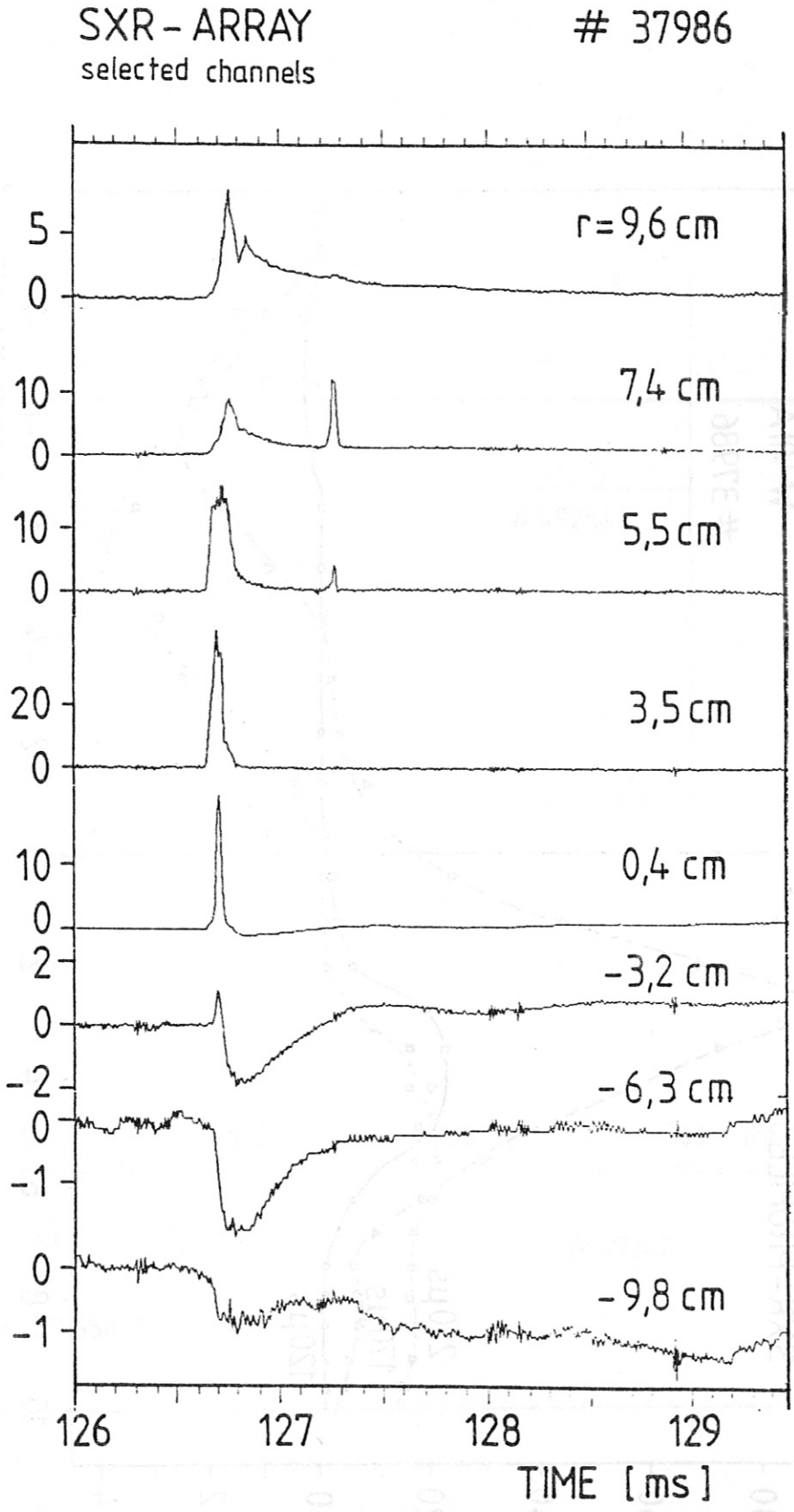
SXR - ARRAY
selected channels
# 37986
r = 9,6 cm
7,4 cm
5,5 cm
3,5 cm
0,4 cm
-3,2 cm
- 6,3 cm
- 9,8 cm
5
0
10
0
10
0
20
0
10
0
2
0
-2
0
-1
0
-1
126
127
128
129
TIME [ms]

Figure 23

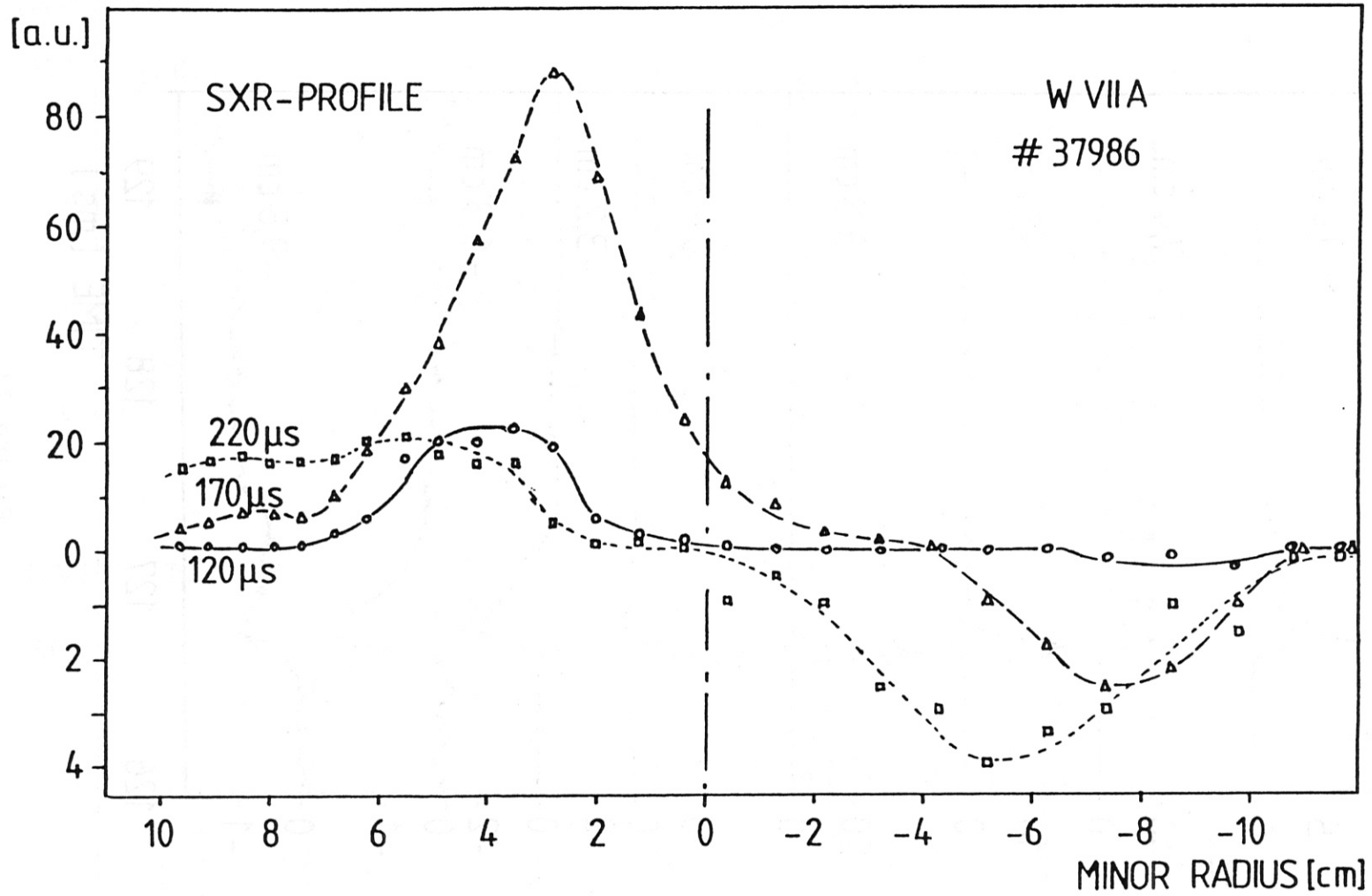
[a.u.]
SXR-PROFILE
W VII A
37986
220 µs
170 µs
120 µs
80
60
40
20
0
2
4
10
8
6
4
2
0
-2
-4
-6
-8
-10
MINOR RADIUS [cm]

Figure 24

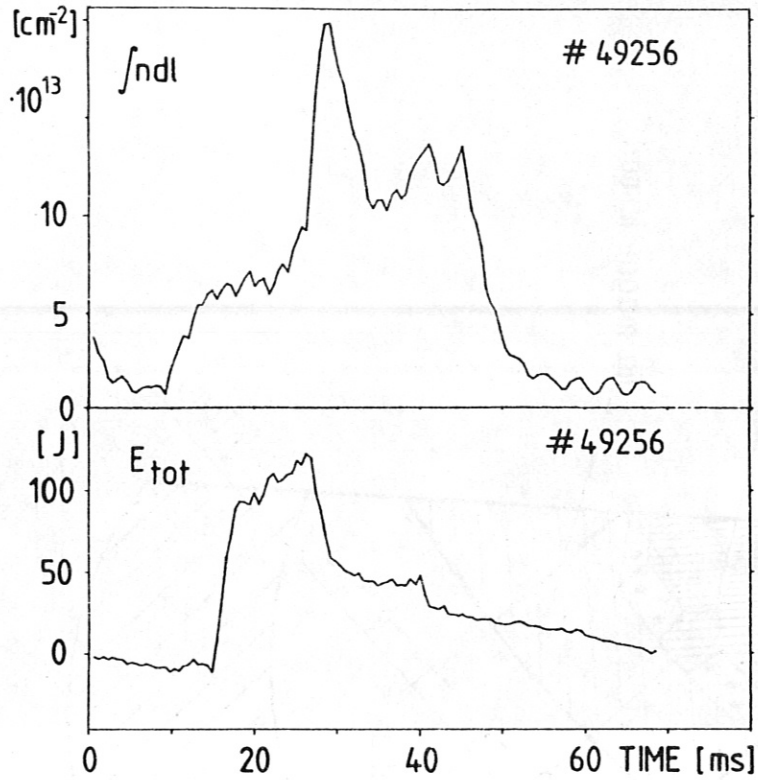

Figure 25

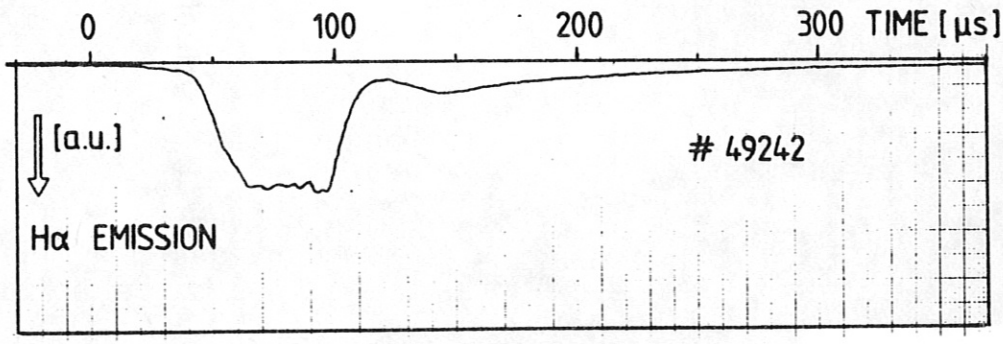

Figure 26

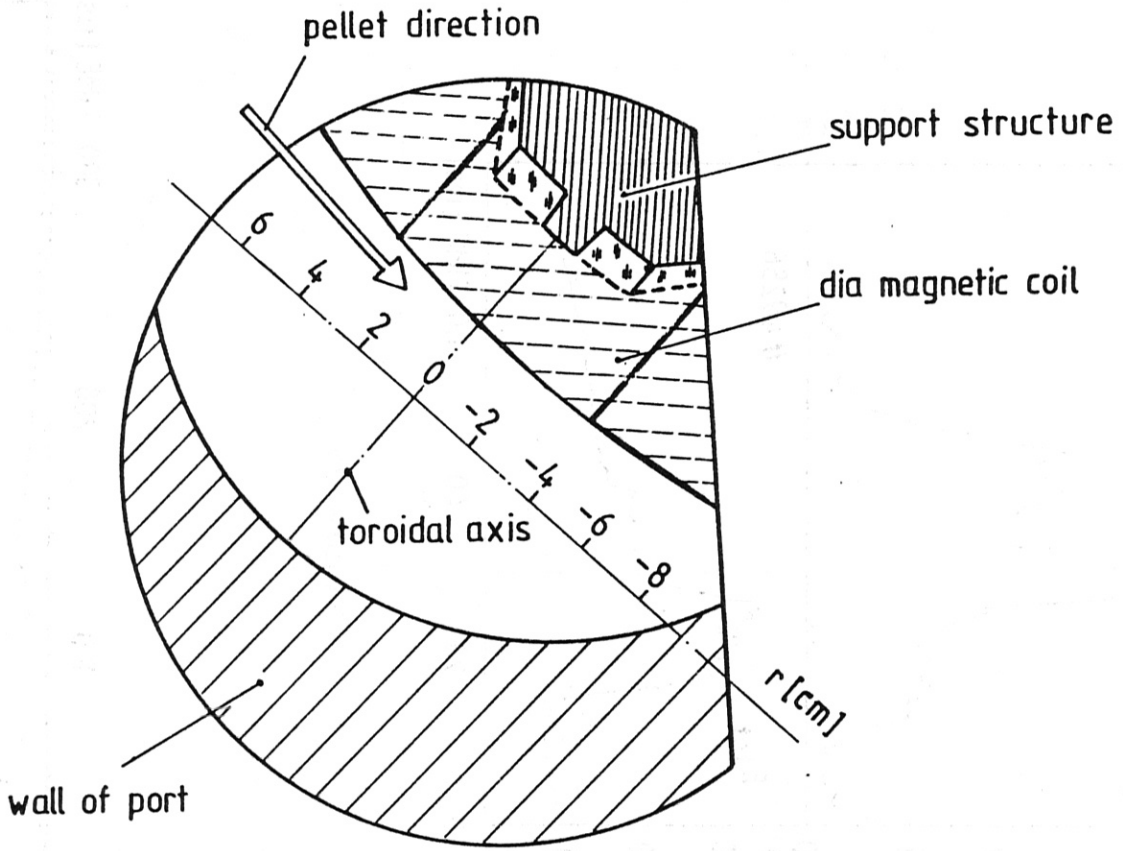
pellet direction
support structure
dia magnetic coil
6
4
2
0
-2
-4
-6
-8
toroidal axis
r[cm]
wall of port

Figure 27

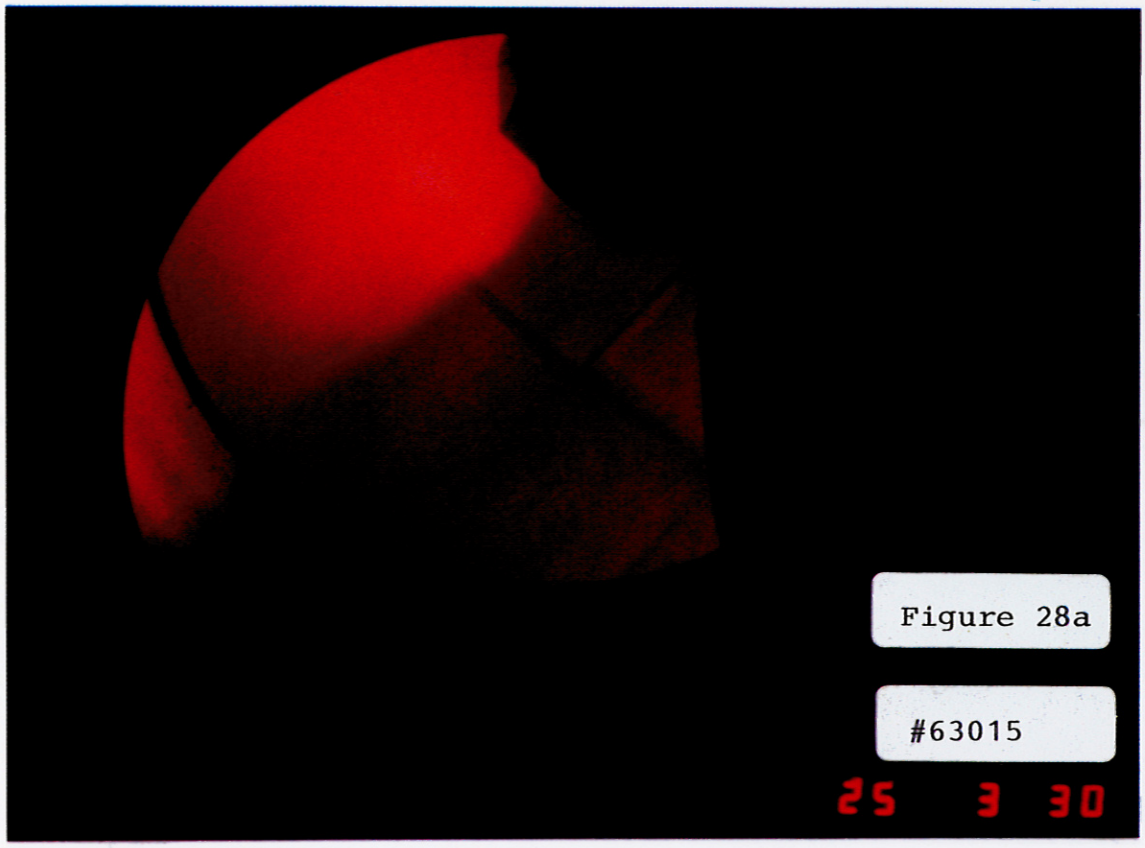
Figure 28a
#63015
25 3 30

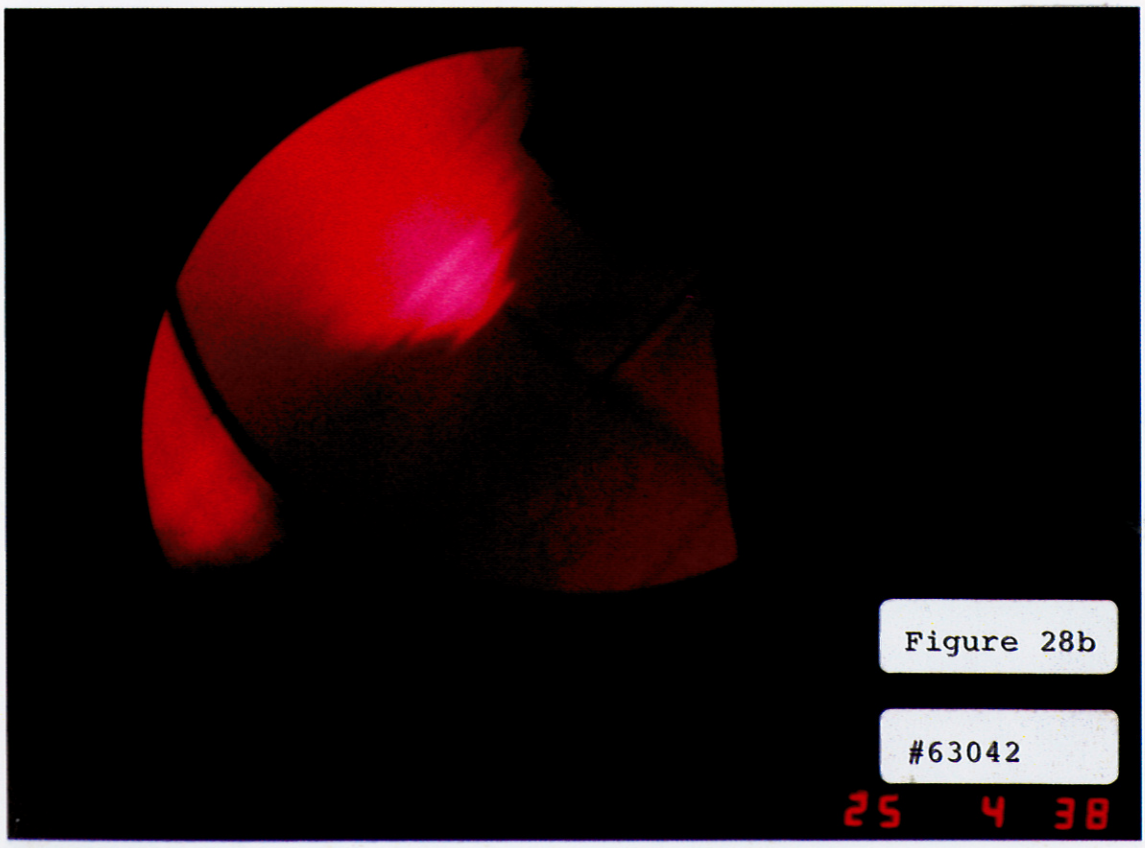
Figure 28b
#63042
25 4 38

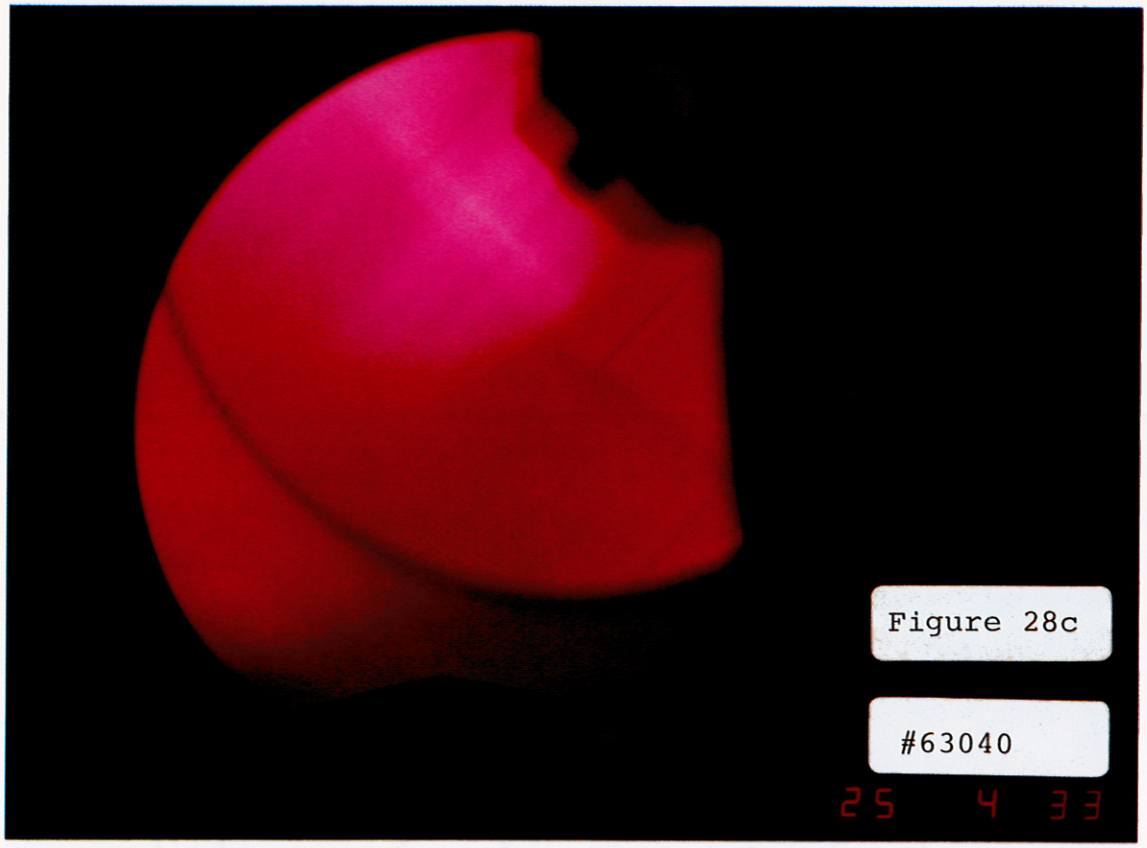
Figure 28c
#63040
25 4 33

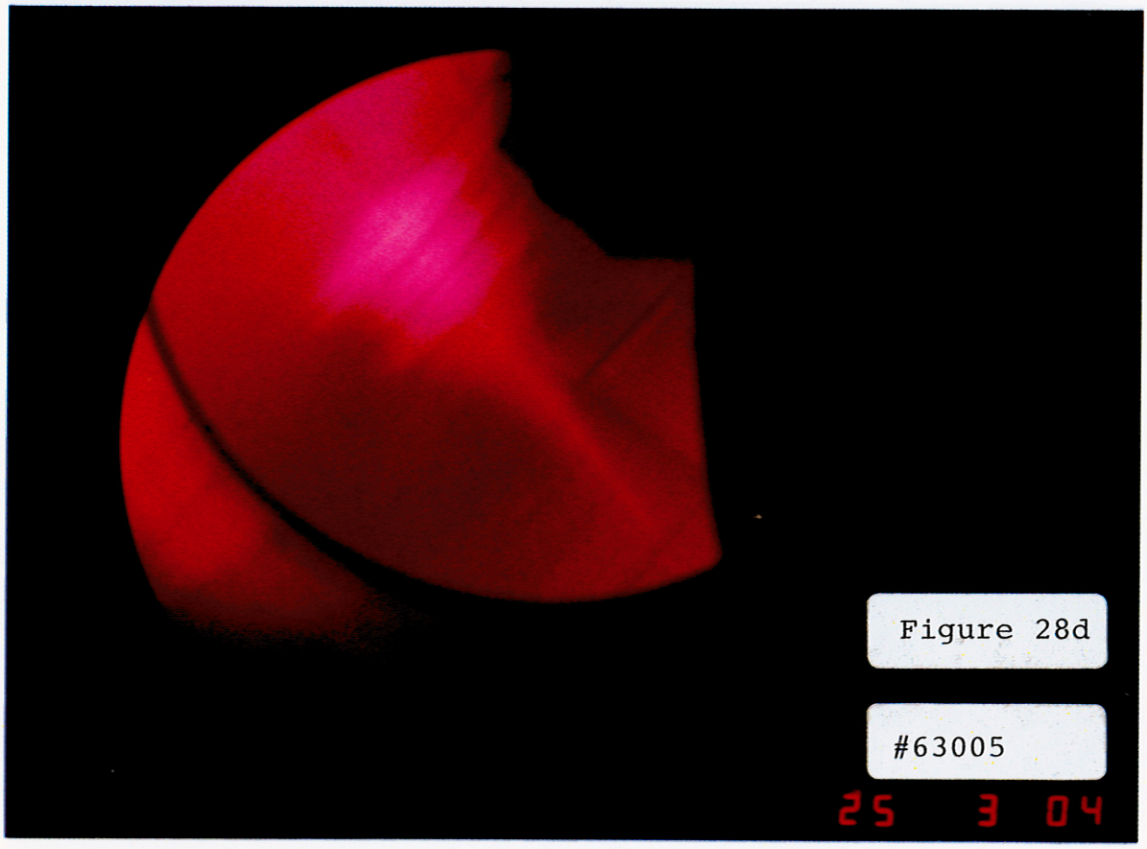
Figure 28d
#63005
25 3 04

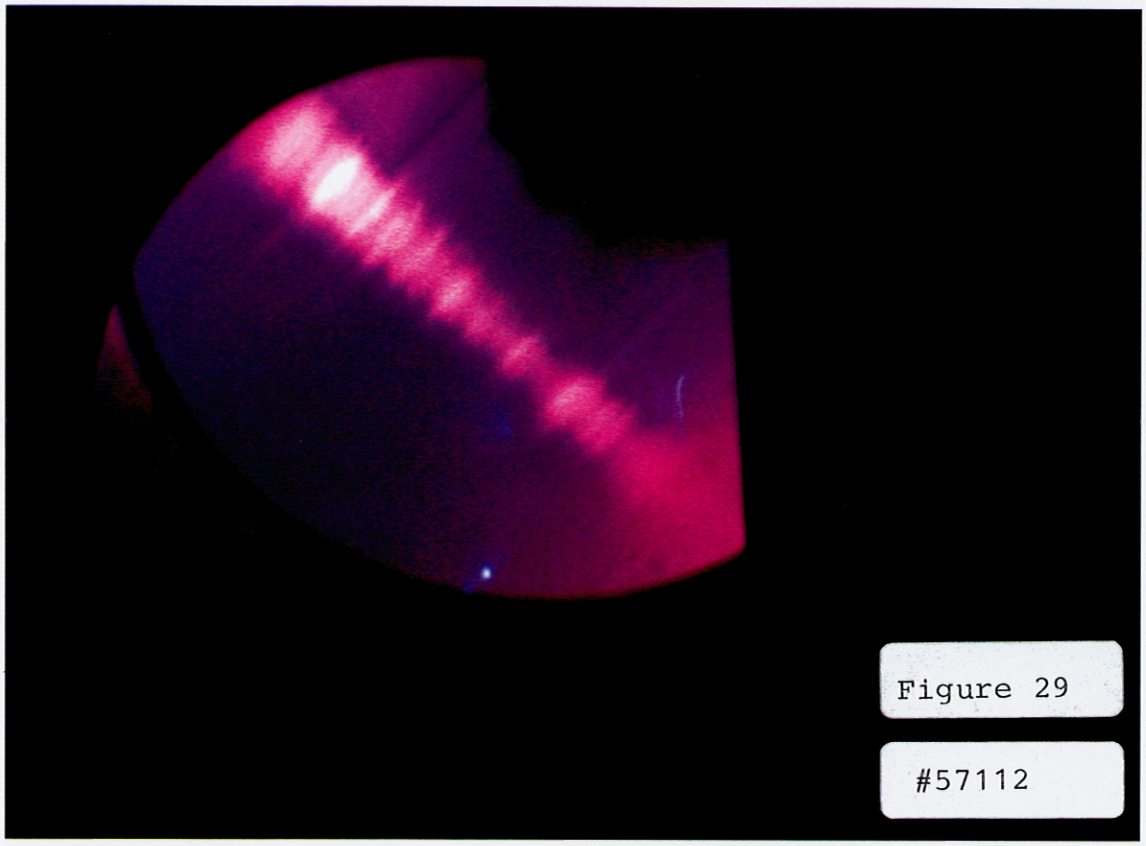

Figure 29

#57112

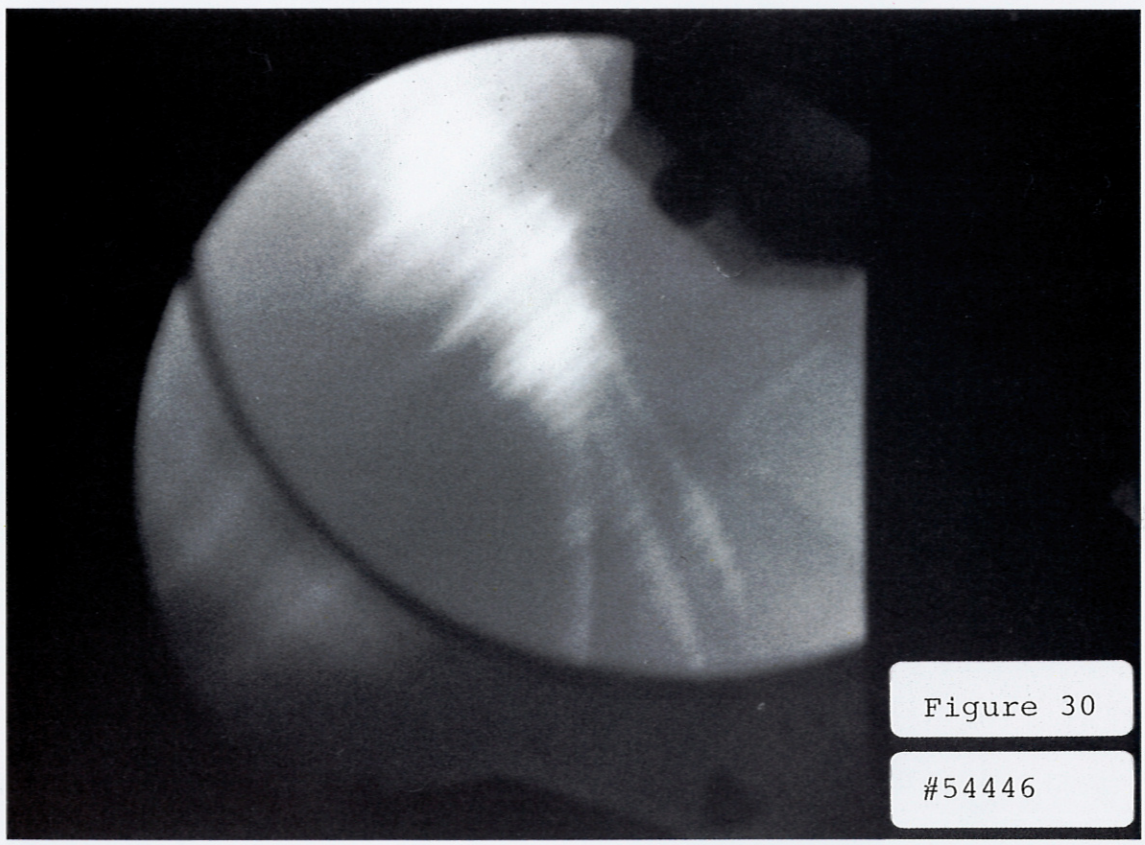

Figure 30

#54446